IEEE Access
Multidisciplinary ⋮ Rapid Review ⋮ Open Access Journal

Received 8 April 2026, accepted 18 May 2026, date of publication 21 May 2026, date of current version 28 May 2026.

Digital Object Identifier 10.1109/ACCESS.2026.3695607

RESEARCH ARTICLE

Volatility-Aware Sizing and Seasonally Adaptive Control of Hybrid Energy Storage Using Multi-Horizon Forecasting in a Nordic Campus Microgrid

TAREQ ANWAR SHIKDAR[1] **AND HANNU LAAKSONEN**[1,2,3]**, (Member, IEEE)**
[1]School of Technology and Innovations, University of Vaasa, 65200 Vaasa, Finland
[2]School of Technology and Innovations, Flexible Energy Resources Team, University of Vaasa, 65200 Vaasa, Finland
[3]Department of Electrical Engineering, University of Vaasa, 65200 Vaasa, Finland

Corresponding author: Hannu Laaksonen (hannu.laaksonen@uwasa.fi)

ABSTRACT The electrification of heating, transportation, and buildings is transforming modern campuses into multi-energy environments where photovoltaic (PV) generation, electric-vehicle (EV) fast charging, and heat-pump (HP) loads interact across multiple timescales. These interactions introduce high volatility that conventional battery energy storage systems (BESS) and short-horizon forecasting techniques cannot manage effectively, particularly in Nordic climates with extreme seasonal irradiance and heating-dominated load patterns. This study develops a unified analytical–AI–optimization framework for sizing and controlling a hybrid battery energy storage system (HBSS) that integrates a fast-response supercapacitor/lithium titanate (SC/LTO) layer with a Li-ion energy storage layer. Volatility is quantified using three indicators: the PV Volatility Index (PVI), EV Fast-Charging Impact Factor (EFI), and Thermal Load Flexibility Index (TLFI) derived from a 3.5-year, 15-minute dataset from a Nordic university campus microgrid. A multi-horizon deep-learning model (HERA-4C), combining convolutional blocks, BiLSTM layers, and attention mechanisms, produces 1-, 4-, 24-, and 96-step forecasts and is embedded into a predictive energy-management and multi-objective optimization scheme using NSGA-II. The five-objective formulation minimizes annualized cost, CO_2 emissions, grid import, Li-ion degradation, and unmet load. Results indicate that the optimal HBSS configuration (≈260 kW SC/LTO and 200 kWh Li-ion) mitigates over 90% of PV–EV–HVAC volatility, reduces peak grid import by 72%, eliminates curtailment and unmet load, and achieves 15–22% annual cost reduction alongside a 14–18% decrease in CO_2 emissions. Seasonal evaluation confirms enhanced winter reliability through adaptive state-of-charge management. The proposed framework provides a reproducible methodology for resilient HBSS design in operational campus microgrids and supports scalable smart-building applications under high-volatility conditions.

INDEX TERMS Hybrid BESS, volatility modeling, multi-horizon forecasting, predictive control, NSGA-II optimization, campus microgrid, seasonal operation.

I. INTRODUCTION

The rapid electrification of buildings, transportation, and heating systems is fundamentally reshaping modern distribution networks. University and institutional campuses are transitioning from passive load centers into complex multi-energy environments where photovoltaic (PV) generation, electric-vehicle (EV) charging infrastructure, and electrically driven heating, ventilation, and air-conditioning (HVAC) systems interact dynamically on the same electrical feeder [1]. While this transition supports decarbonization and energy-efficiency objectives, it simultaneously introduces

The associate editor coordinating the review of this manuscript and approving it for publication was Arturo Conde.

significant operational volatility across multiple time scales, challenging conventional planning, forecasting, and energy management strategies [2].

PV generation is a primary contributor to short-term volatility due to its sensitivity to irradiance fluctuations. Cloud-edge effects and rapidly changing weather conditions can cause steep PV power ramps within minutes or even seconds, particularly in Nordic and temperate climates. These high-frequency variations propagate directly into the distribution network, affecting power quality and increasing the need for fast-acting flexibility resources. In parallel, the growing penetration of EV fast chargers, typically rated between 150 and 350 kW, introduces step-like load changes that can severely stress local feeders and transformers when multiple charging events coincide [3], [4], [5]. EV charging behavior is inherently stochastic and closely tied to user mobility patterns, making it difficult to predict and manage using traditional load models.

Electrified heating further compounds this challenge. Heat pumps, which are increasingly deployed to replace fossil-fuel-based heating systems, exhibit electrical demand that varies strongly with ambient temperature, compressor cycling, and defrost operations. In cold climates, the coefficient of performance (COP) of heat pumps can fluctuate widely, with reported winter values often ranging between 1.1 and 2.5 [6]. Large-scale field studies have shown that even systems exposed to similar outdoor conditions may exhibit substantial performance differences, leading to mid-frequency power fluctuations that interact with both PV generation and EV charging demand [7]. The combined effect of PV ramps, EV fast-charging surges, and heat-pump-driven variability results in a multi-sector volatility profile that cannot be adequately addressed using single-timescale forecasting or conventional energy storage approaches.

Accurate forecasting and flexible energy storage are therefore essential for reliable and economical campus microgrid operation. Recent advances in deep-learning-based forecasting have significantly improved short-term prediction of PV output and building loads [8], with convolutional neural networks (CNNs), recurrent neural networks (RNNs), and long short-term memory (LSTM) models outperforming traditional statistical techniques such as ARIMA and regression-based approaches [9]. Hybrid architectures that combine convolutional layers with recurrent units and attention mechanisms have demonstrated strong performance in capturing nonlinear temporal dependencies [8], [9], [10]. However, most existing studies focus on a single signal type (e.g., PV or load), consider limited forecast horizons (typically 1–4 steps ahead), or evaluate forecasting accuracy in isolation without embedding predictions into operational energy management or storage control frameworks [11].

Battery energy storage systems (BESS) play a central role in mitigating volatility, enabling peak shaving, energy shifting, and grid support in microgrids. Conventional lithium-ion (Li-ion) batteries are widely deployed due to their high energy density and declining costs, yet they are poorly suited for absorbing high-frequency power fluctuations such as PV ramps or EV fast-charging transients. Frequent high C-rate operation accelerates electrochemical degradation and shortens battery lifetime, undermining both economic and operational performance [12], [13], [14]. To overcome these limitations, hybrid battery energy storage systems (HBSS), which combine fast-response technologies such as supercapacitors or lithium-titanate (LTO) cells with energy-oriented Li-ion batteries, have gained increasing attention. Such hybrid architectures allow rapid power disturbances to be buffered by the fast layer, while the Li-ion layer handles medium-duration energy balancing and load following [13], [14].

Despite growing interest in hybrid storage systems and advanced forecasting techniques, several critical gaps remain in the existing literature. First, many studies investigating hybrid battery architectures rely on synthetic demand profiles or short-duration simulation datasets rather than long-term measured operational data. For example, previous works such as [15] evaluate hybrid storage coordination under simulated load conditions but do not explicitly relate measured volatility from PV generation, EV charging demand, and HVAC-driven thermal loads to storage power–energy partitioning. As a result, the interaction between sector-coupled demand variability and hybrid storage control remains insufficiently explored.

Second, although significant progress has been made in energy forecasting methods, these models are rarely integrated directly into operational storage dispatch frameworks. Several forecasting studies focus primarily on prediction accuracy without embedding the forecasts within real-time energy management strategies. For instance, works such as [16] develop predictive models for renewable generation, while studies including [17] and [18] explore load forecasting techniques; however, the resulting predictions are typically used only for evaluation purposes rather than as direct inputs to hybrid storage control. Consequently, coordinated decision-making based on multi-horizon forecasts—from short-term volatility mitigation to day-ahead planning—remains limited.

Third, seasonal asymmetry is frequently overlooked in existing hybrid storage studies. In Nordic energy systems, electricity demand patterns exhibit strong seasonal variation, characterized by significant PV surplus during summer months and heating-dominated demand during winter periods. However, many storage management strategies assume static operational policies throughout the year, as reported in [18], which limits their ability to adapt to seasonal variability and changing system dynamics.

Finally, comprehensive multi-objective optimization frameworks that simultaneously consider economic cost, CO_2 emissions, grid interaction, battery degradation, and supply reliability remain relatively scarce in the literature. Existing studies such as [6], [7], and [8] typically focus

on a limited set of objectives, such as cost minimization or emission reduction, while works including [17] and [18] analyze operational strategies under simplified assumptions. Few studies combine long-term high-resolution operational datasets with integrated forecasting and hybrid storage optimization, leaving an important gap in the development of unified decision-support frameworks for modern microgrid systems.

To address these challenges, this paper proposes a unified, forecast-driven, volatility-aware hybrid energy storage framework for campus microgrids. The proposed approach integrates:

- Sector-coupled volatility quantification using normalized indices derived from PV, EV, and heat-pump ramp dynamics
- A deep-learning-based multi-horizon forecasting model capable of producing consistent predictions from 15 minutes to 24 hours ahead.
- A hybrid supercapacitor/LTO–Li-ion battery energy storage system optimized and controlled using a five-objective NSGA-II formulation. Seasonal state-of-charge (SOC) trajectories are explicitly incorporated to reflect the asymmetric operating conditions of Nordic climates.

The framework is validated using a 3.5-year, 15-minute-resolution dataset from a real university campus microgrid in Vaasa, Finland, encompassing PV generation, building electrical load, EV charging demand, heat-pump operation, electricity market prices, and grid CO_2 intensity. By embedding multi-horizon forecasts directly into hybrid storage dispatch and optimization, the proposed method demonstrates significant reductions in peak grid import, operating cost, CO_2 emissions, and Li-ion battery degradation, while maintaining zero unmet load across all seasons.

The remainder of this paper is organized as follows. Section II reviews related work on sector-coupled volatility, multi-horizon forecasting, hybrid energy storage systems, and microgrid optimization. Section III presents the proposed methodology, including volatility indices, forecasting integration, hybrid storage modeling, and optimization formulation. Section IV describes the dataset and system model. Sections V–VII present forecasting results, hybrid storage operation, and optimization outcomes. Section VIII discusses robustness, sensitivity, and practical implications, and Section IX concludes the paper with key findings and future research directions.

II. LITERATURE REVIEW

This section reviews prior research relevant to sector-coupled volatility in campus microgrids, multi-horizon forecasting techniques, hybrid battery energy storage systems, and multi-objective optimization approaches. The discussion highlights methodological limitations in existing studies and establishes the motivation for the integrated framework proposed in this paper.

A. SECTOR-COUPLED VOLATILITY IN CAMPUS MICROGRIDS

PV output in Nordic and Central European climates changes rapidly when clouds move across the array. Field measurements show sharp ramps that appear within seconds or minutes, indicating that flexibility across multiple time scales is required [17], [18]. Lindholm and Jokinen documented this behavior in Finnish rooftop systems; the recorded swings were large enough to matter for both forecasting and storage planning [19]. Converter dynamics can amplify inevitable fluctuations as MPPT behavior does not respond linearly [20]. While statistical variability models exist [21], [22], most storage sizing studies still rely on long-term averages [23] and therefore miss the implications of high-frequency PV ramps. Fast charging introduces a different type of stress. Chargers in the 150–350 kW class create sudden load steps that affect feeder voltage and protection schemes [24]. Recent NERC assessments show that groups of EV chargers can rapidly push currents upward, stressing distribution components [25]. Similar findings appear in local studies where coincident charging has been shown to overload distribution transformers within short periods [26]. Even so, EV surge characteristics are rarely linked to sizing requirements for the fast-response part of a hybrid storage system. Heat pumps add mid-frequency variability. Ambient temperature, frosting events, and compressor cycling strongly influence their electrical input. COP measurements in Nordic climates vary widely, typically ranging from 1.1 to 2.5, depending on conditions [27]. Larger datasets show that two systems exposed to the same temperature may still produce very different COP values, sometimes by a factor of two or more [7]. This behavior affects SOC trajectories and increases sensitivity to forecasting errors, yet many microgrid studies treat HP operation in overly simplified ways.

B. MULTI-HORIZON FORECASTING FOR MICROGRID OPERATION

Deep-learning models now dominate short- and medium-term forecasting tasks. They generally outperform earlier statistical approaches such as ARIMA and SVR [8]. Several hybrid architectures have emerged, including CNN–LSTM models for multi-horizon load forecasting [28], CNN–Transformer combinations for PV prediction [29], and attention mechanisms that adjust forecasts to changing weather patterns [30]. Nevertheless, most of the existing work still focuses on either PV or load alone. Forecast horizons beyond 24 steps are seldom considered, and only a small number of studies attempt to link forecasts to real-time hybrid storage control. Forecast uncertainty is also rarely included in seasonally varying dispatch decisions. As a result, the forecasting and optimization processes remain largely disconnected.

C. HYBRID BATTERY ENERGY STORAGE SYSTEMS

Hybrid battery energy storage system (BESS) designs often combine fast-response devices—typically supercapacitors or lithium-titanate (LTO) cells—with conventional Li-ion batteries to balance power density and energy capacity. Recent review studies, such as [15], highlight the advantages of these hybrid architectures in systems exposed to rapid fluctuations and frequent cycling, where high-power devices can absorb short-term disturbances while Li-ion batteries handle longer-duration energy balancing. In practical implementations, case studies such as [31] demonstrate that hybrid configurations improve transient response and reduce degradation stress on Li-ion batteries by offloading high-frequency power variations to the fast-response layer.

Despite these advances, several important gaps remain in the literature. First, most existing studies focus primarily on operational benefits or control strategies, but few works propose systematic sizing approaches that directly link measured volatility characteristics of renewable generation and demand to the required power and energy capacities of the hybrid storage layers. Second, although multi-objective optimization methods have been applied in energy system design, their use in hybrid storage sizing and coordinated control remains relatively limited. For example, studies such as [32] investigate optimization of energy storage systems under simplified operating conditions, while [33] focuses on operational scheduling strategies without explicitly incorporating forecasting information. Finally, many of these studies rely on synthetic load profiles or short-term simulation datasets, which makes it difficult to generalize their findings to real campus-scale energy systems with long-term operational variability.

D. MULTI-OBJECTIVE OPTIMIZATION IN MICROGRIDS

Multi-objective optimization has become an essential tool for microgrid planning and operational decision making because energy systems inherently involve conflicting technical, economic, and environmental objectives. Evolutionary algorithms such as NSGA-II are widely adopted in this context due to their ability to efficiently explore nonlinear, nonconvex design spaces and generate well-distributed Pareto-optimal solutions without requiring gradient information. These characteristics make NSGA-II particularly suitable for complex microgrid problems where multiple operational constraints, stochastic renewable generation, and heterogeneous energy resources must be considered simultaneously.

However, most existing NSGA-II-based microgrid studies remain relatively simplified in their problem formulation. Typical implementations focus on a single storage technology and optimize only two objectives, most commonly economic cost and CO_2 emissions. Furthermore, many studies rely on annual-average or synthetic demand profiles, which neglect short-term operational dynamics and fail to capture the multi-timescale variability introduced by renewable generation and emerging electrified loads.

In modern campus microgrids, operational complexity has increased significantly due to the strong coupling between photovoltaic generation, electric-vehicle fast charging, and electrically driven heating systems such as heat pumps. These components introduce volatility across multiple temporal scales, ranging from second-level PV ramp events to hourly thermal load fluctuations and day-ahead demand variability. Addressing these dynamics requires optimization frameworks that simultaneously consider multiple operational objectives—including cost, emissions, grid import, battery degradation, and reliability—while explicitly modeling hybrid storage architectures and time-varying system behavior.

Despite substantial progress in the literature on PV variability, EV charging impacts, heat-pump dynamics, forecasting models, and hybrid battery systems, these research areas are often investigated in isolation. Forecasting studies typically focus on prediction accuracy without integrating forecasts into operational optimization, while storage studies frequently assume simplified or deterministic load profiles. As a result, forecasting, hybrid storage design, and operational optimization remain largely disconnected in many existing microgrid frameworks.

Existing forecasting-driven energy management and hybrid storage studies have demonstrated improvements in renewable integration, operational scheduling, and predictive storage coordination using forecasting, optimization, and artificial intelligence techniques [8], [28], [29], [30], [15], [31], [32], [33], [34], [35]. However, many existing approaches focus primarily on either forecasting accuracy, operational dispatch, or single-sector energy variability independently. In addition, several studies rely on simplified load representations, short-duration simulation datasets, or static operational policies that do not fully capture the coupled variability introduced by photovoltaic generation, EV fast charging, and heat-pump-driven thermal demand under highly seasonal Nordic operating conditions. In contrast, the proposed framework integrates sector-coupled volatility characterization, multi-horizon forecasting, uncertainty-aware hybrid SC/LTO–Li-ion dispatch, seasonally adaptive SOC management, and multi-objective optimization within a unified framework validated using long-term real campus operational data.

To address these limitations, the present study employs NSGA-II as a robust multi-objective search mechanism within a unified optimization framework that integrates sector-coupled volatility analysis, multi-horizon forecasting, and hybrid battery energy storage system (HBSS) modeling. Unlike conventional formulations, the proposed approach jointly optimizes the sizing and operation of fast-response SC/LTO storage and energy-oriented Li-ion batteries while accounting for multi-year high-resolution operational data, seasonal demand asymmetry, and forecasting-informed dispatch decisions. In this context, NSGA-II serves as an

enabling optimization backbone that allows exploration of the trade-offs between economic performance, environmental impact, grid interaction, battery lifetime, and supply reliability under realistic campus microgrid operating conditions.

E. TRANSFORMER AND FRACTIONAL-ORDER LEARNING APPROACHES IN ENERGY FORECASTING

Recent advancements in renewable energy forecasting have increasingly leveraged deep learning architectures to address the nonlinear and highly volatile nature of renewable generation and demand. Traditional recurrent and convolutional neural networks, such as LSTM, BiLSTM, and CNN-based models, have demonstrated strong performance in short-term forecasting tasks [8], [28], [29], [30]. However, their ability to capture long-range temporal dependencies and multi-scale patterns remains limited. To overcome these limitations, transformer-based architectures have recently gained significant attention in renewable energy forecasting [34]. These models utilize self-attention mechanisms to capture global temporal dependencies and complex interactions across time steps. The core operation of a transformer model is defined as:

$$\text{Attention}\,(Q, K, V) = \text{softmax}\left(\frac{QK^T}{\sqrt{d_k}}\right)V \tag{1}$$

where Q, K, and V represent query, key, and value matrices, respectively, and d_k is the dimensionality of the key vector. This formulation enables parallel processing and improved representation of long-range temporal correlations, making transformer-based models particularly effective for multi-horizon forecasting tasks [34], [35].

In addition to transformer models, hybrid and memory-enhanced learning approaches have been proposed to improve forecasting accuracy under non-stationary conditions. One such approach is the fractional-order recurrent neural network (FRNN), which incorporates long-term memory effects using fractional calculus [40]. The Caputo fractional derivative is commonly used to model such dynamics:

$${}^{C}D_t^{\alpha} f\,(t) = \frac{1}{\Gamma\,(1-\alpha)} \int_0^t (t-\tau)^{-\alpha} f'\,(\tau)\,d\tau \tag{2}$$

This formulation allows the model to capture history-dependent system behavior, which is particularly relevant for photovoltaic systems and load patterns influenced by long-term temporal correlations [6], [7]. In practice, the fractional derivative is often approximated using the Grünwald–Letnikov scheme:

$$\Delta_h^{\alpha} y_k \approx h^{-\alpha} \sum_{j=0}^{L} \omega_j^{(\alpha)} y_{k-j} \tag{3}$$

These hybrid and fractional-order models have shown promising results in improving prediction accuracy and robustness under uncertain operating conditions [34].

Despite these advancements, transformer-based and fractional-order models often require large-scale datasets, high computational resources, and complex parameter tuning, which may limit their applicability in real-time energy management systems [34], [35]. Furthermore, most existing works focus primarily on forecasting accuracy without integrating the predictions into operational decision-making frameworks.

In contrast, the proposed HERA-4C framework adopts a hybrid CNN–BiLSTM–attention architecture that balances predictive accuracy with computational efficiency. More importantly, it integrates multi-horizon forecasting directly with hybrid energy storage system optimization, enabling a unified forecasting–control pipeline for practical energy management applications.

F. RESEARCH GAP AND MOTIVATION

Based on the reviewed literature, several critical research gaps can be identified:

- Existing studies lack a unified framework that jointly considers PV generation, EV fast charging, and heat-pump-driven thermal loads using long-term, high-resolution campus data.
- Multi-horizon forecasting, particularly spanning from minutes to day-ahead operation within a single consistent model, is rarely integrated into microgrid control and storage dispatch.
- There is no systematic methodology for linking measured volatility to hybrid storage power–energy partitioning, especially for fast-response and energy-oriented storage layers.
- Seasonal asymmetry, which is fundamental to Nordic and other high-latitude climates, is often neglected in both storage sizing and control strategies.
- Comprehensive multi-objective optimization frameworks that simultaneously account for economic cost, CO_2 emissions, grid import, battery degradation, and reliability under real operational conditions remain limited.

These gaps motivate the development of an integrated, forecasting-driven, volatility-aware hybrid energy storage framework. By combining sector-coupled volatility indices, deep-learning-based multi-horizon forecasting, hybrid SC/LTO–Li-ion battery modeling, and five-objective NSGA-II optimization, this paper aims to provide a scalable and reproducible solution for resilient campus microgrid operation under high-volatility conditions.

Although recent forecasting-assisted energy management system (EMS) studies have improved renewable integration and storage scheduling performance, most existing approaches focus on either single-sector variability, short-term forecasting horizons, or operational dispatch without explicitly linking measured volatility characteristics to hybrid storage sizing and seasonal operational adaptation. Furthermore, many existing frameworks evaluate forecasting and storage control independently, limiting coordinated decision-making under highly dynamic operating

conditions. In contrast, the proposed framework integrates sector-coupled volatility characterization, multi-horizon forecasting, uncertainty-aware hybrid SC/LTO–Li-ion dispatch, and seasonally adaptive SOC management within a unified optimization framework validated using long-term real operational data from a Nordic campus microgrid. The proposed methodology additionally establishes a quantitative relationship between measured volatility behavior and hybrid storage power–energy partitioning, enabling coordinated sizing and operation of fast-response and energy-oriented storage layers.

G. DISTINCT CONTRIBUTIONS OF THIS PAPER

Compared with existing forecasting-assisted hybrid energy management and storage optimization studies, the distinct contributions of this paper are summarized as follows:

- This work introduces a unified volatility characterization framework that explicitly captures the coupled dynamics of photovoltaic generation, electric-vehicle fast charging, and heat-pump-driven thermal loads using long-term, high-resolution campus data. Three normalized volatility indices are formulated to translate measured ramp behavior into actionable storage design inputs.
- A deep-learning-based multi-horizon forecasting model is developed to generate consistent predictions from 15 minutes to 24 hours ahead within a single architecture. Unlike conventional single-horizon approaches, these forecasts are directly embedded into hybrid energy storage dispatch, enabling predictive and horizon-aware control.
- The proposed framework establishes a quantitative link between measured system volatility and hybrid storage power–energy partitioning, enabling systematic sizing of a fast-response SC/LTO layer and an energy-oriented Li-ion layer. This approach moves beyond heuristic or simulation-only hybrid storage design.
- A season-dependent state-of-charge (SOC) control strategy is introduced to explicitly address the asymmetric operating conditions of Nordic climates, characterized by summer PV surplus and winter heating-dominated demand. This ensures improved reliability and reduces stress on the Li-ion battery across all seasons.
- A five-objective NSGA-II optimization framework is formulated to jointly minimize annualized cost, CO_2 emissions, grid import, battery degradation, and unmet load. The optimization incorporates forecasting-driven dispatch and hybrid storage dynamics, yielding Pareto-optimal designs under realistic operational constraints.
- The proposed methodology is validated using a 3.5-year, 15-minute-resolution dataset from a real university campus microgrid in Vaasa, Finland. The results demonstrate substantial reductions in peak grid import, operating cost, CO_2 emissions, and Li-ion degradation while maintaining zero unmet load across all seasons.

III. METHODOLOGY

This section describes the proposed forecasting-driven, volatility-aware hybrid energy storage methodology developed for campus microgrids. The methodology integrates sector-coupled volatility analysis, multi-horizon forecasting, hybrid battery energy storage system (HBSS) modeling, seasonal state-of-charge (SOC) control, and multi-objective optimization.

A. OVERALL FRAMEWORK DESCRIPTION

The proposed framework follows a predictive energy management paradigm in which measured system volatility and multi-horizon forecasts jointly inform hybrid storage sizing and dispatch decisions. The methodology consists of five sequential stages:

- Extraction and normalization of volatility from PV generation, EV charging, and heat-pump-driven thermal loads.
- Generation of short- and long-horizon forecasts using a unified deep-learning model
- Hybrid storage dispatch modeling with fast and slow dynamic separation.
- Seasonally adaptive SOC trajectory enforcement
- Multi-objective optimization of storage sizing and operational parameters.

The interaction between these stages is illustrated in Figure. 1. Forecast outputs feed directly into the energy management system (EMS), while volatility indices constrain hybrid storage power–energy partitioning. Figure 1 shows the interaction between volatility extraction, multi-horizon forecasting, hybrid BESS dispatch, seasonal SOC control, and NSGA-II optimization. Forecasts and volatility indices jointly inform real-time and long-term storage decisions.

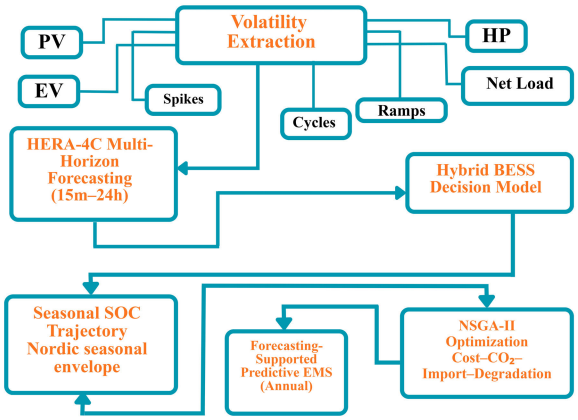

FIGURE 1. Overview of the proposed volatility-aware forecasting–optimization framework for hybrid energy storage operation in campus microgrids.

B. VOLATILITY QUANTIFICATION AND NORMALIZATION

Operational volatility is quantified through ramp-rate analysis of sector-coupled power signals. Let $P_k(t)$ denote the instantaneous power of the subsystem $k \in \{\text{PV}, \text{EV}, \text{HP}$

at time step t, sampled at an interval Δt. The ramp rate is defined as

$$R_k(t) = \frac{P_k(t) - P_k(t - \Delta t)}{\Delta t}. \quad (4)$$

To enable consistent comparison across subsystems with different nominal ratings, normalized volatility indices are introduced.

The PV Volatility Index (PVI) is defined as

$$\mathrm{PVI} = \frac{\sigma(|R_{\mathrm{PV}}|)}{P_{\mathrm{PV}}^{\max}}, \quad (5)$$

The EV Fast-Charging Impact Factor (EFI) as

$$\mathrm{EFI} = \frac{\sigma(|R_{\mathrm{EV}}|)}{P_{\mathrm{EV}}^{\max}}, \quad (6)$$

and the Thermal Load Flexibility Index (TLFI) as

$$\mathrm{TLFI} = \frac{\sigma(|R_{\mathrm{HP}}|)}{P_{\mathrm{HP}}^{\max}}, \quad (7)$$

where $\sigma(\cdot)$ denotes the standard deviation of absolute ramp rates. These indices characterize the relative intensity of fast and mid-frequency disturbances and are used to guide hybrid storage sizing and dispatch. Figure 2 illustrates how raw power measurements are converted into ramp-rate distributions and normalized volatility indices used for hybrid storage design

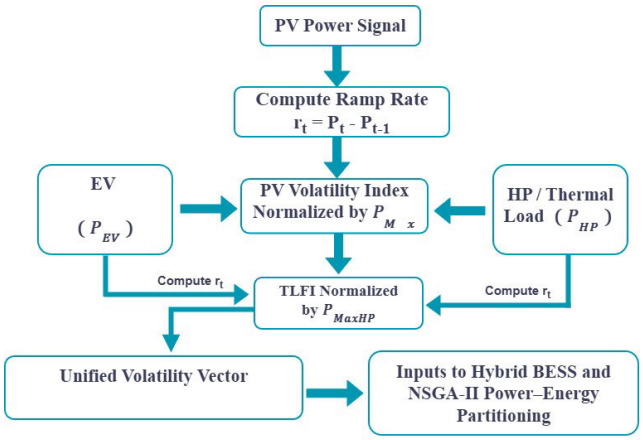

FIGURE 2. Volatility extraction and normalization process for PV, EV charging, and heat-pump loads.

C. MULTI-HORIZON FORECASTING AS PREDICTIVE INPUT

Multi-horizon forecasts of PV generation and net load are generated using a unified forecasting model. At each time step t, the model produces a forecast vector

$$\hat{P}(t) = \left\{\hat{P}(t+1), \hat{P}(t+4), \hat{P}(t+24), \hat{P}(t+96)\right\} \quad (8)$$

corresponding to prediction horizons of 15 min (Fast volatility mitigation), 1 h (Short-term dispatch smoothing), 6 h (Energy shifting), and 24 h (Seasonal SOC planning, respectively. Short-horizon forecasts are primarily used to mitigate rapid power fluctuations, while long-horizon forecasts support anticipatory charging, price-aware scheduling, and seasonal SOC planning. Forecasts are updated in a rolling-horizon manner to limit error propagation.

The proposed HERA-4C forecasting architecture is designed to balance predictive accuracy and computational efficiency for practical energy management system (EMS) applications. Training is performed offline using historical operational data, where the convolutional, BiLSTM, and attention layers jointly learn multi-timescale temporal patterns. Although the training phase requires higher computational resources due to iterative parameter optimization, this process is executed only periodically during model retraining and does not affect real-time operation. In contrast, online inference during EMS deployment is computationally lightweight, as forecast generation involves only a forward-pass evaluation of the trained model. The rolling-horizon forecasting process can therefore be executed within operational EMS timescales, enabling practical integration into real-time hybrid storage dispatch and predictive energy management frameworks. Furthermore, the unified multi-horizon architecture reduces the need for multiple independent forecasting models, improving deployment efficiency and simplifying operational implementation for campus-scale microgrids.

1) MULTI-HORIZON OUTPUT LAYER AND LOSS FUNCTION

The HERA-4C forecasting model is designed to produce simultaneous predictions across multiple horizons using a shared feature representation. Let the multi-horizon forecast output be defined as:

$$\hat{P}(t) = \left[\hat{P}_{t+1}, \hat{P}_{t+h_1}, \hat{P}_{t+h_2}, \ldots, \hat{P}_{t+h_n}\right] \quad (9)$$

where each component corresponds to a specific prediction horizon. These outputs are generated through a shared encoder–decoder architecture, ensuring that temporal dependencies across horizons are jointly learned.

To enforce consistency across different prediction horizons, the model is trained using a combined multi-horizon loss function:

$$\mathcal{L} = \sum_{i=1}^{n} w_i \cdot MSE\left(\hat{P}_{t+h_i}, P_{t+h_i}\right) \quad (10)$$

where w_i represents the weighting factor for horizon h_i, and MSE denotes the mean squared error between predicted and actual values.

This formulation ensures that all horizons are optimized simultaneously while allowing flexible prioritization of short-term or long-term accuracy. The shared representation across horizons inherently promotes temporal consistency, preventing divergence between short- and long-term predictions

2) UNCERTAINTY-AWARE DISPATCH FORMULATION

To enhance robustness against forecast uncertainty, the dispatch formulation is extended to incorporate a confidence-adjusted control strategy. Although the primary dispatch is

based on point forecasts obtained from the multi-horizon model, forecast uncertainty is accounted for through a safety margin applied to predicted values.

The uncertainty-adjusted net load is defined as:

$$P_{\text{adj}}(t) = P_{\text{forecast}}(t) - k \cdot CI_h(t) \tag{11}$$

where $CI_h(t)$ represents the forecast confidence interval width at time t for horizon h, and k is a tuning parameter that controls the level of conservativeness. The forecast confidence interval width is derived using a residual-based uncertainty estimation approach. During model validation, prediction residuals are calculated as the difference between forecasted and measured values for each forecasting horizon. The standard deviation of these residuals is then used to estimate the forecast uncertainty level associated with each prediction horizon. Assuming approximately symmetric forecast error behavior, the confidence interval width is expressed as:

$$CI_h(t) = z_\alpha \sigma_h \tag{12}$$

where:

- $CI_h(t)$ = confidence interval width for horizon h
- z_α = confidence coefficient
- σ_h = standard deviation of forecasting residuals for horizon h

This formulation ensures that the dispatch strategy remains robust against forecast errors, particularly under high-volatility conditions. By incorporating uncertainty into the control input, the system reduces the likelihood of constraint violations and improves operational reliability. In addition, the adaptive threshold $R_{th}(t, s)$, defined in Eq. (9), is directly linked to forecast confidence intervals, enabling the hybrid storage system to respond more conservatively when uncertainty is high. This effectively introduces a chance-constrained behavior in the dispatch mechanism without requiring a full stochastic optimization framework.

D. HYBRID BATTERY ENERGY STORAGE DISPATCH MODEL

The hybrid energy storage system consists of a fast-response supercapacitor/lithium titanate (SC/LTO) layer and an energy-oriented Li-ion battery. The SC/LTO layer is intentionally designed with a high power-to-energy ratio to address short-duration, high-frequency disturbances associated with photovoltaic ramp events, EV fast-charging transients, and rapid thermal-load fluctuations. Unlike energy-oriented Li-ion batteries, the primary function of the SC/LTO subsystem is not long-duration energy shifting but rapid power buffering and transient stabilization. Consequently, a relatively small energy capacity combined with a high power rating is adopted to enable fast charge/discharge response, high cycling capability, and reduced electrochemical stress on the Li-ion layer. The Li-ion battery subsequently manages slower and longer-duration energy balancing requirements, thereby enabling functional separation between fast transient mitigation and medium-duration energy management within the hybrid storage architecture. The net power imbalance between load and photovoltaic (PV) generation is defined as

$$P_{\text{net}}(t) = P_{\text{load}}(t) - P_{\text{PV}}(t) \tag{13}$$

To separate fast and slow dynamics, a ramp-based power-splitting strategy is adopted. The ramp rate is defined as

$$R(t) = \frac{P_{\text{net}}(t) - P_{\text{net}}(t - \Delta t)}{\Delta t} \tag{14}$$

High-frequency components are assigned to the SC/LTO layer based on a threshold $R_{th}(t, s)$:

$$P_{\text{SC}}(t) = \begin{cases} P_{\text{net}}(t), & |R(t)| > R_{th}(t, s) \\ 0, & \text{otherwise} \end{cases} \tag{15}$$

Unlike a fixed threshold, $R_{th}(t, s)$ is implemented as a seasonally initialized but dynamically updated parameter:

$$R_{th}(t, s) = \alpha VI_s + \beta CI_h(t) \tag{16}$$

where VI_s represents the combined seasonal volatility index derived from the normalized PVI, EFI, and TLFI indicators, and $CI_h(t)$ denotes the forecast confidence interval width obtained from the multi-horizon forecasting model at time t for horizon h. The coefficients α and β control the relative influence of historical volatility and real-time forecast uncertainty. This formulation enables adaptive sensitivity, allowing the fast-response layer to react more aggressively under high volatility or high uncertainty conditions.

The Li-ion battery handles the residual power after fast-component extraction:

$$P_{\text{Li}}(t) = P_{\text{net}}(t) - P_{\text{SC}}(t) \tag{17}$$

State-of-charge (SOC) dynamics for both storage layers are governed by:

$$\text{SOC}_i(t+1) = \text{SOC}_i(t) + \frac{\eta_i P_i(t) \Delta t}{E_i^{\max}}, \quad i \in \{\text{SC}, \text{Li}\} \tag{18}$$

To ensure physically feasible operation under prolonged volatility events, a hierarchical fallback mechanism is incorporated. When the SC/LTO layer approaches its SOC or power limits, any remaining high-frequency imbalance is transferred to the Li-ion battery, subject to its operational constraints. If both storage layers reach their limits, the residual mismatch is handled through grid import/export or curtailed according to network constraints. This hierarchical control structure ensures stable system operation while preventing saturation of the fast-response layer and excessive stress on the Li-ion battery. Figure 3 shows how fast disturbances are absorbed by the SC/LTO layer while the Li-ion battery handles slower energy balancing.

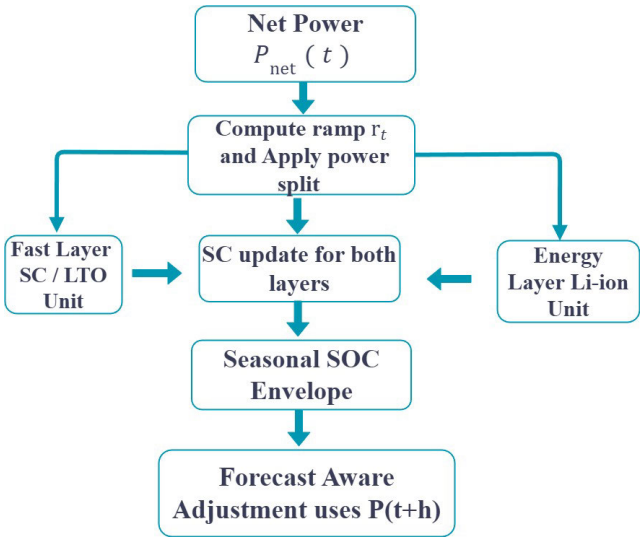

FIGURE 3. Hybrid SC/LTO–Li-ion power-splitting and energy flow structure.

E. BATTERY DEGRADATION MODELLING

To incorporate battery aging into the optimization framework, a simplified cycle-based degradation model is adopted. The degradation of the Li-ion battery is assumed to be primarily driven by charge–discharge cycling, which is consistent with its operational role in medium-duration energy balancing. The degradation cost is modeled as a function of energy throughput:

$$C_{\text{deg}} = \lambda \sum_{t} | P_{\text{Li}}(t) | \Delta t \tag{19}$$

where λ represents the degradation cost coefficient (€/kWh throughput), and $| P_{\text{Li}}(t) |$ is the absolute Li-ion power. This formulation approximates cycle-induced degradation by penalizing cumulative energy throughput.

This approach captures the dominant aging mechanism under frequent cycling conditions, where depth-of-discharge and charge/discharge activity are the primary contributors to capacity fade. The use of a throughput-based model is consistent with widely adopted simplified degradation formulations in energy system optimization. Calendar aging and temperature-dependent degradation effects are not explicitly modeled in this study, which represents a limitation of the adopted simplified degradation framework. In practical battery systems, temperature variations, long-term storage conditions, and electrochemical side reactions can significantly influence aging behavior and lifetime degradation characteristics. However, the primary objective of the present work is to evaluate the operational impact of hybrid storage coordination and volatility-aware dispatch under varying campus microgrid conditions rather than to develop a detailed electrochemical battery aging model. Therefore, a throughput-based degradation representation is adopted to provide computationally efficient comparative evaluation of hybrid storage operation and Li-ion cycling stress within the multi-objective optimization framework. Future work may extend the proposed methodology by incorporating temperature-coupled electrochemical degradation models, calendar aging mechanisms, and rainflow-cycle-based lifetime estimation techniques.

F. SEASONALLY ADAPTIVE SOC CONTROL

To account for strong seasonal asymmetry, season-dependent SOC bounds are imposed on the Li-ion battery:

$$\text{SOC}_{\min} \leq \text{SOC}_{\text{Li}}(t) \leq \text{SOC}_{\max}, \tag{20}$$

where $s \in \{\text{Winter, Spring, Summer, Autumn}\}$. The seasonal SOC bounds were selected based on the observed seasonal mismatch between photovoltaic generation and campus electrical demand within the 2021–2025 operational dataset. Higher SOC targets are maintained during winter periods to preserve reserve capacity against heating-driven demand variability, reduced photovoltaic availability, and increased forecast uncertainty under Nordic climatic conditions. In contrast, lower SOC ranges are permitted during summer periods to maximize photovoltaic self-consumption and reduce renewable curtailment during high solar generation conditions. The adopted SOC envelopes were additionally evaluated through preliminary operational sensitivity observations to ensure stable hybrid storage operation, avoidance of excessive Li-ion cycling stress, and sufficient flexibility across varying seasonal demand conditions. Although the SOC thresholds are not derived from a dedicated optimization process, they provide a practically interpretable and operationally robust strategy for seasonally adaptive hybrid storage management within the studied campus microgrid.

G. MULTI-OBJECTIVE OPTIMIZATION FORMULATION

Hybrid storage sizing and operational parameters are optimized using NSGA-II. The decision vector is

$$\mathbf{x} = \{E_{\text{Li}}, P_{\text{Li}}^{\max}, P_{\text{SC}}^{\max}\}. \tag{21}$$

Optimization minimizes

$$\min_{\mathbf{x}} \begin{bmatrix} C_{\text{ann}} \\ \text{CO}_2 \\ E_{\text{import}} \\ D_{\text{Li}} \\ E_{\text{unserved}} \end{bmatrix}, \tag{22}$$

subject to SOC, power, and reliability constraints. Figure 4 illustrates population initialization, fitness evaluation, non-dominated sorting, and convergence toward the Pareto front.

H. PERFORMANCE EVALUATION METRICS

System performance is assessed using forecasting accuracy metrics (RMSE, R^2, Diebold–Mariano test), operational indicators (volatility absorption ratio, peak grid import, SOC adherence), and long-term economic and environmental metrics.

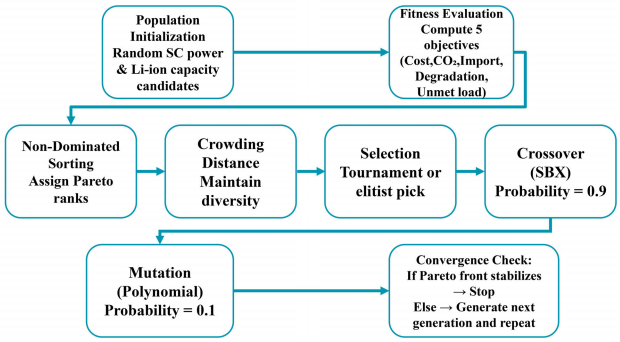

FIGURE 4. NSGA-II optimization workflow for hybrid storage sizing and dispatch.

IV. SIMULATION MODEL DESIGNING AND STRUCTURING

A. DATA SOURCES AND PREPROCESSING

The study is based on a unified dataset representing a real campus microgrid at the University of Vaasa, Finland, covering the period 2021–2025 with a 15-minute temporal resolution (1492 days). The dataset integrates electrical demand, photovoltaic (PV) generation, electric-vehicle (EV) charging demand, thermal load, weather conditions, electricity market prices, and grid CO_2 intensity. All electrical and PV measurements were collected through the campus Energy Management System (EMS) and follow IEC 61724-1 monitoring practices [15]. Power meters are Class-1 certified. EV charging power data was obtained from OCPP-compliant chargers, ensuring accurate logging of charging sessions and power levels. Weather variables, including ambient temperature, global horizontal irradiance, wind speed, and humidity, were retrieved from the NASA POWER database [36]. EV data were obtained from Data in brief [37] Electricity market prices were obtained from the ENTSO-E Transparency Platform [38], while time-varying grid CO_2 intensity data were sourced from the Fingrid Open Data Service [39]. Data preprocessing involved three steps. First, all signals were synchronized to a common 15-minute timestamp. Second, missing values accounting for less than 0.7% of the dataset were reconstructed using linear interpolation. Third, outliers caused by logging or communication errors were removed using a 3σ statistical filter. The resulting dataset provides a consistent basis for forecasting, volatility quantification, and hybrid storage optimization.

B. CAMPUS MICROGRID CONFIGURATION

The studied system represents a grid-connected campus microgrid located at the University of Vaasa, Finland. The microgrid integrates multiple energy subsystems including photovoltaic (PV) generation, building electrical demand, electric-vehicle (EV) charging infrastructure, an electrified heating system based on heat pumps, and a hybrid battery energy storage system (BESS). A centralized energy management system (EMS) coordinates these components and manages energy flows within the campus network.

In operation, electricity generated by the PV system is first used to satisfy local building demand and EV charging loads. When excess renewable generation is available, the surplus energy can be stored in the hybrid BESS or exported to the utility grid. Conversely, during periods of high demand or low renewable production, electricity can be imported from the grid. The hybrid BESS provides operational flexibility by separating fast power disturbances and medium-duration energy balancing through a combination of SC/LTO and Li-ion storage layers.

The main technical parameters of the PV system, EV charging infrastructure, HVAC system, hybrid BESS, and dataset characteristics are summarized in Table 1, which provides an overview of the campus microgrid configuration and the data sources used in the study.

TABLE 1. Dataset overview and sources (2021–2025, 15-min resolution).

Component	Parameter	Value	Source
PV System	Installed capacity	870 kWp	Energy Lab - buildings (2021–2025)
	Inverter efficiency	97.5%	Fronius Symo datasheet [44]
EV Chargers	4 × DC fast chargers	150 kW each	Open EV dataset scaled to campus [40]
	20 × AC Level 2 chargers	11 kW each	Open EV dataset [40]
HVAC	Air-to-water heat pump	550 kW	Energy Lab - building's thermal logs
	COP (winter/summer)	2.0 / 4.1	NIBE F2120 datasheet [43]
Hybrid BESS	SC/LTO power rating	260 kW	HBSS design specification [43]
	SC energy	3.2 kWh	HBSS design specification [43]
	Li-ion energy	200 kWh	BYD LVL datasheet [45]
Dataset	Resolution	15 minutes	IEC 61724-1 standard [46]
	Duration	1492 days	Unified merged dataset (2021–2025)

Table I summarizes the main components, technical parameters, and data sources used in the unified campus-scale dataset. The dataset integrates photovoltaic generation, electric vehicle charging infrastructure, HVAC systems, and a hybrid battery energy storage system (HBESS), covering the period 2021–2025 with a uniform 15-min temporal resolution. Technical specifications are obtained from manufacturer datasheets, building energy management systems, and standardized datasets, while operational profiles are harmonized in accordance with IEC 61724-1. The resulting dataset provides a consistent and high-resolution basis for energy system modeling, optimization, and performance evaluation

C. VALIDATION OF SCALED EV CHARGING PROFILE

The EV charging dataset used in this study is derived from an open-source EV charging dataset [37] and scaled to match

the installed charging infrastructure of the campus microgrid. To ensure that the scaled dataset accurately represents realistic campus charging behavior, a statistical validation is performed. First, the peak charging power levels are consistent with the installed infrastructure, which includes multiple DC fast chargers rated at 150 kW and AC chargers rated at 11 kW. The aggregated EV charging profile reflects realistic peak demand levels observed in campus environments. Second, the temporal variability and ramp-rate characteristics of the scaled EV data are analyzed. The ramp-rate distribution, shown in Figure. 7, indicates that EV charging events exhibit step-like variations with ramp magnitudes typically within ±8–10 kW per 15-minute interval. These characteristics are consistent with stochastic charging behavior reported in campus and urban EV studies. Third, the statistical dispersion of EV charging demand, including standard deviation and variability patterns, aligns with reported EV usage trends, where charging events are intermittent and user-driven rather than continuous.

Although the dataset is scaled, these statistical properties confirm that it preserves the key characteristics relevant for volatility analysis, particularly ramp behavior and peak coincidence effects. Therefore, the scaled EV dataset provides a representative approximation of campus-level EV charging dynamics for hybrid storage design and evaluation.

D. DATASET STRUCTURE AND MULTI-SECTOR LOAD PROFILES

The dataset includes synchronized time series of building electrical load, PV production, EV charging demand, heat-pump consumption, electricity market prices, grid CO_2 intensity, and key meteorological variables. Figure 4 presents the combined load and PV power over the full period 2021–2025.

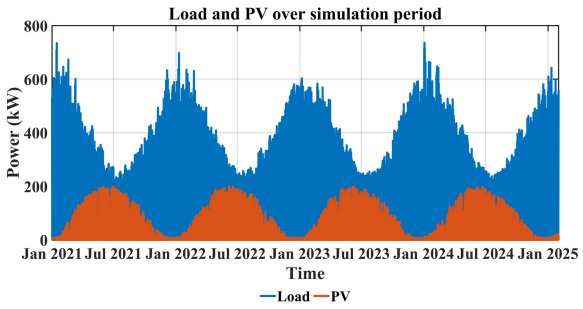

FIGURE 5. Load and PV over the full simulation period (2021–2025).

Figure 5 shows a pronounced seasonal pattern. PV generation increases sharply during summer, often reaching values close to 200 kW, while winter production drops to near zero due to low irradiance and snow cover. In contrast, building load peaks during winter, rising to two to three times summer levels due to heating demand. This structural mismatch, with high PV output in summer and high load in winter, is characteristic of Nordic buildings and has been reported in earlier studies [16], [17]. The seasonal imbalance reinforces the need for a hybrid BESS configuration capable of providing both short-term volatility mitigation and seasonally adaptive SOC management.

E. LOAD DECOMPOSITION: BASE LOAD, EV CHARGING, AND HEAT PUMP

The full load decomposition for the period 2021–2025 is illustrated in Fig. 6, where the total building demand is expressed as:

$$P_{\text{load}}(t) = P_{\text{base}}(t) + P_{\text{EV}}(t) + P_{\text{heat}}(t) \tag{23}$$

Fig. 6 presents the load components using separate panels for heat-pump demand, EV charging demand, and base electrical load, allowing clearer visualization of their temporal characteristics.

The heat-pump demand (Figure. 6(a)) exhibits strong seasonal variation, with pronounced peaks during winter months driven by low ambient temperatures and continuous heating requirements. During these periods, it dominates the total demand and typically accounts for a significant portion of peak load.

In contrast, EV charging demand (Figure. 6(b)) appears as intermittent and irregular peaks associated with fast-charging sessions. These events are short-duration but high-power, reflecting typical usage patterns in campus environments with increasing EV penetration.

The base electrical load (Figure. 6(c)) remains comparatively stable throughout the year, representing underlying building consumption such as lighting, appliances, and auxiliary systems. Although minor fluctuations are observed, its magnitude is significantly less variable than the heat-pump component.

Overall, the distinct temporal characteristics of these components highlight the multi-sector coupling and variability of modern campus energy systems. These observations are consistent with measured profiles in Nordic academic and commercial buildings [38], confirming the representativeness of the dataset used in this study

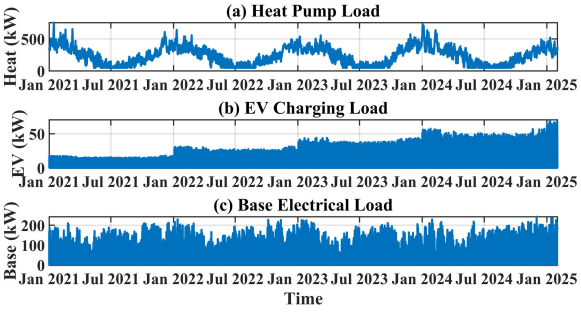

FIGURE 6. Load decomposition into base load, EV charging, and heat pump (2021–2025).

F. VOLATILITY METRICS (PVI, EFI, TLFI)

Figure. 7 presents the ramp-rate histograms for PV generation, EV charging, and heat-pump operation across the

2021–2025 dataset. Following the ramp-characterization method of Kazemi et al. [44], three sector-specific volatility measures are defined in equations (2), (3), and (4).

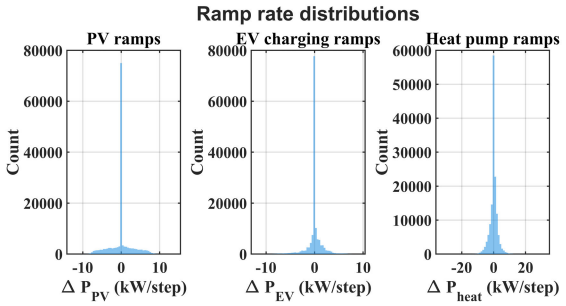

FIGURE 7. Ramp-rate histograms for PV, EV charging, and heat pump power.

The three histograms reveal apparent differences in ramp behavior. PV generation exhibits step changes mostly within ±10–12 kW per 15-minute interval, reflecting typical cloud movements in coastal Nordic climates. EV charging shows a narrower range with occasional swings of approximately ±8–10 kW/step, produced by the sudden start and end of fast-charging sessions. Heat-pump operation exhibits the widest distribution: most ramps fall within ±15 kW/step, but occasional excursions exceed ±25–30 kW/step during compressor restarts and defrost cycles. These characteristics have direct implications for hybrid storage design PVI determines the fast-response rating required from the SC/LTO layer, EFI affects transient absorption capability, and TLFI influences the Li-ion layer sizing for multi-minute thermal fluctuations.

G. SPATIOTEMPORAL PATTERNS VIA HEATMAPS

Fig. 8(a–d) displays annual 365 × 24 heatmaps of load, PV generation, grid power, and BESS SOC following the method of [45]. The load heatmap (Fig. 8a) shows a strong seasonal gradient, with winter demand dominating and pronounced morning (06–09) and evening (17)–(21) peaks linked to heating and occupancy. Summer loads are substantially lower. PV output (Fig. 8b) exhibits a clear seasonal envelope, concentrated between 07–18 and peaking around midday, with negligible production during winter. Grid power (Fig. 8c) reflects the interaction of load and PV availability: summer midday periods exhibit negative values indicating exports, whereas winter is characterized by persistent imports driven by heating loads. The BESS SOC (Figure. 8d) stays above ∼0.75 for most of the year, rising toward the upper bound during summer due to midday PV charging, and showing tight oscillations in winter as the control strategy preserves reserve capacity for volatility mitigation. Overall, the heatmaps reveal the coupled diurnal–seasonal dynamics of demand, renewable generation, grid exchange, and storage behavior in the campus microgrid.

H. SEASONAL ENERGY BALANCE

Table 2 reveals a pronounced seasonal imbalance between renewable generation and electricity demand.

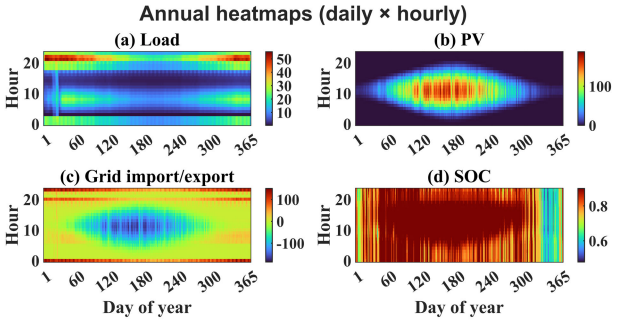

FIGURE 8. Spatiotemporal heatmaps of load, PV, grid power, and SOC.

Winter operation is characterized by very low PV output (31,834 kWh) and high heating-driven demand (208,820 kWh), resulting in substantial grid imports. In contrast, spring and summer exhibit significant PV surpluses (380–488 MWh), leading to grid exports exceeding 340 MWh and 450 MWh, respectively, while autumn shows intermediate behavior with moderate PV production and import-dominated operation.

TABLE 2. Seasonal energy summery.

Season	PV (kWh)	Load (kWh)	Import (kWh)	Export (kWh)
Winter	31,834	208,820	199,450	21,253
Spring	380,120	145,910	110,430	344,130
Summer	487,820	90,668	55,688	452,140
Autumn	108,710	141,050	118,760	85,664

Table II presents the aggregated seasonal energy balance of the campus energy system over the 2021–2025 period. Seasonal totals of photovoltaic (PV) generation, electrical load demand, grid electricity import, and surplus energy export are reported in kilowatt-hours. The results highlight the strong seasonal variability in PV production and grid interaction, with peak PV generation and export occurring during summer months, while winter operation is characterized by higher load demand and increased grid imports

These results confirm the structural mismatch typical of Nordic climates, where renewable availability peaks in summer while demand is highest in winter. The proposed hybrid BESS directly mitigates this mismatch by assigning short-term volatility from PV ramps, EV charging, and heat-pump cycling to the SC/LTO layer, while the Li-ion battery provides medium-term energy balancing. Seasonally adaptive SOC control further preserves sufficient reserves during winter and maximizes utilization of PV surplus during summer. Building on this characterization of temporal and volatility dynamics, the following section applies the HERA-4C forecasting model to generate multi-horizon predictions that support hybrid storage decision-making.

V. SIMULATION MODEL DESIGNING AND STRUCTURING

A 6 × 96 sliding window (24 h of historical data at 15-min resolution) is used as model input. The selected features

capture the dominant physical, operational, and environmental drivers of pv and load volatility in Nordic climates, including electrical signals, weather conditions, market indicators, co_2 intensity, and temporal features. The complete feature set and preprocessing steps are summarized in Table 3.

TABLE 3. Input features and preprocessing steps.

Feature Group	Variables Included	Preprocessing Applied
Electrical signals	Load, PV, grid import/export	Z-score normalization, missing-value interpolation
Weather variables	Ambient temperature, GHI/irradiance, wind speed	Z-score normalization
Market/CO_2 signals	Electricity price, CO_2 intensity	Z-score normalization
Time indicators	Hour, day, month, weekday/weekend, season label	One-hot or cyclic encoding
Derived features	Ramp rates, lag terms, rolling statistics	Standard normalization

Table iii summarizes the input feature groups and corresponding preprocessing steps applied prior to model training. Electrical, weather, and market-related variables are normalized to ensure numerical stability and balanced feature scaling, while missing values are addressed through interpolation. Temporal indicators are encoded using one-hot or cyclic representations to preserve periodic patterns, and additional derived features, including ramp rates, lagged variables, and rolling statistics, are incorporated to enhance the model's ability to capture short- and medium-term dynamics.

All continuous variables are normalized using z-score scaling following established forecasting practice [46], [47], [48]. Missing values (<0.1% of the dataset) are corrected using forward interpolation, consistent with PV-integrated microgrid recommendations [49].

A. HERA-4C ARCHITECTURE

The HERA-4C model integrates four complementary components:

- Captures local temporal patterns such as PV ramps, EV charging transitions, and heat-pump cycling (Convolutional encoder).
- Models long-range temporal dependencies, including diurnal and weekly structure (Bi-directional LSTM).
- Highlights high-impact time steps (e.g., sunrise/sunset, EV arrivals- Scaled dot-product attention).
- Simultaneously generates forecasts for h = 1, 4, 24, 96 within a unified multi-task framework (multi-head horizon projection layer).

Full architecture is illustrated in the figure. 9.

HERA-4C introduces three key innovations over existing approaches [50], [51], [52], [53]:

I. Joint multi-horizon learning within a single architecture, avoiding inter-horizon inconsistency.
II. CNN–BiLSTM–attention fusion tailored to high-volatility Nordic microgrids.
III. Direct compatibility with hybrid BESS control, enabling forecasting-driven coordination between SC/LTO and Li-ion layers.

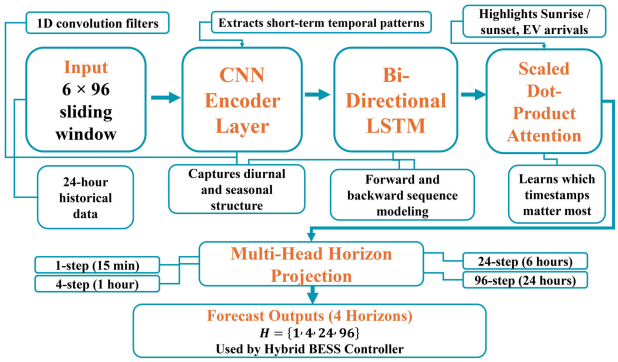

FIGURE 9. HERA-4C architecture block diagram.

B. TRAINING STRATEGY AND BENCHMARK COMPARISON

The model is trained on 143,037 samples from the 2021–2025 dataset using an 80/10/10 train–validation–test split with balanced seasonal coverage. Training employs the Adam optimizer with a learning rate of 1×10^{-3}, batch size 256, and 40 epochs, using Mean Squared Error (MSE) loss. HERA-4C is benchmarked against persistence, ARIMA, LSTM, and CNN models. Table 4 reports performance at the 24-hour horizon, where cumulative volatility is most challenging. HERA-4C achieves the lowest RMSE (0.1628) and highest R^2 (0.9746), reducing RMSE by more than 26% relative to the best baseline (LSTM). These gains are consistent with recent findings [54], [55].

TABLE 4. Baseline forecasting model comparison (24-hour horizon).

Model	$RMSE_{(24)}$	$R^2_{(24)}$
Persistence	0.31	0.82
ARIMA	0.28	0.86
LSTM	0.22	0.92
CNN	0.23	0.91
HERA-4C	**0.1628**	**0.9746**

Table IV compares the 24-hour-ahead forecasting performance of baseline statistical models and data-driven learning approaches using $RMSE_{(24)}$ and $R^2_{(24)}$ as evaluation metrics. The results show progressively improved accuracy with advanced learning models.

C. MULTI-HORIZON FORECASTING PERFORMANCE

Figure. 10 presents representative time-series comparisons between predicted and actual net load for the four forecasting horizons ($H = 1, 4, 24,$ and 96), using a contiguous test window from the evaluation dataset. This visualization enables direct assessment of the model's ability to capture temporal dynamics across multiple time scales.

At the shortest horizon ($H = 1$), the HERA-4C model demonstrates near-perfect tracking of rapid net-load fluctuations driven by photovoltaic (PV) ramping, EV charging

events, and heat-pump cycling. The predicted and actual signals closely overlap, indicating high fidelity in capturing high-frequency dynamics.

At intermediate horizons ($H = 4$ and $H = 24$), the model continues to preserve the underlying temporal structure with minimal phase shift or amplitude distortion. The predictions maintain strong alignment with the actual net load, effectively capturing diurnal patterns and sector-coupled interactions between load and weather-driven components.

At the longest horizon ($H = 96$), the predictions exhibit increased smoothing and moderate deviation from the ground truth, which is expected due to accumulated uncertainty over extended forecast intervals. Nevertheless, the model successfully captures the overall trend and dominant peaks, demonstrating robust learning of long-range temporal dependencies.

Overall, Figure. 10 highlights a controlled and gradual degradation in forecasting accuracy as the horizon increases, without evidence of instability or systematic bias. This behavior is consistent with the quantitative results, where the RMSE increases smoothly from approximately 0.15 at $H = 1$ to 0.28 at $H = 96$, while the coefficient of determination (R^2) remains above 0.93 at the day-ahead horizon. These findings confirm that the proposed HERA-4C framework achieves stable generalization across multiple forecasting horizons, which is essential for reliable downstream energy management and hybrid BESS control.

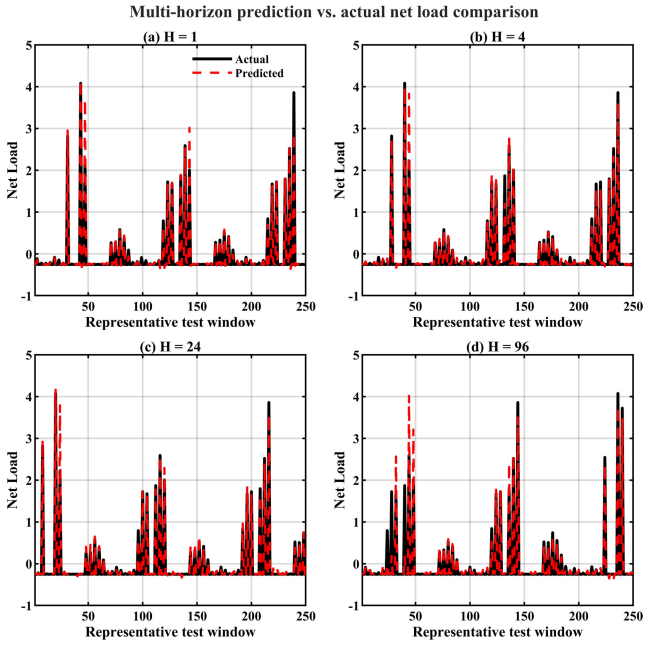

FIGURE 10. Representative comparison between predicted and actual net load across forecast horizons: (a) $H = 1$, (b) $H = 4$, (c) $H = 24$, and (d) $H = 96$.

The parity plots in Figure. 11 further validate these findings, showing tight clustering around the diagonal for H = 1 and H = 4, with moderate dispersion at longer horizons but no observable systematic bias.

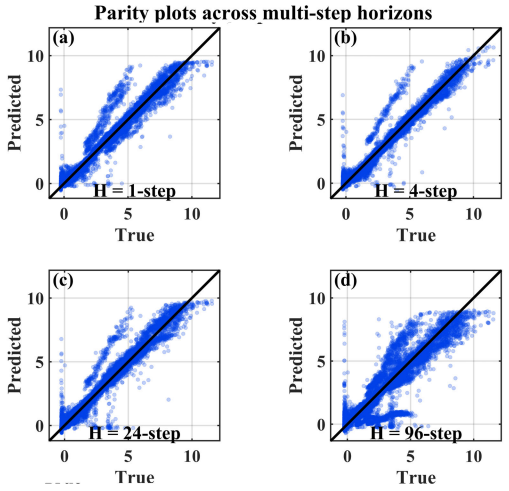

FIGURE 11. Parity plot (H = 1,4,24,96).

D. ABLATION STUDY: PERSISTENCE AND CLIMATOLOGY BENCHMARKS

HERA-4C achieves near-perfect accuracy at short horizons and maintains strong performance at day-ahead prediction (RMSE = 0.282, R^2 = 0.932), exceeding reported results for Nordic microgrids in [56] and [57]. Figure. 12 presents a comprehensive forecast evaluation of the proposed HERA-4C model, including ablation performance, error distributions, and statistical significance tests across multiple horizons (H = 1, 4, 24, 96). In the ablation analysis, HERA-4C consistently outperforms persistence and climatology baselines, maintaining a normalized RMSE below 0.30 and an R^2 exceeding 0.92 at all horizons, while baseline models exhibit flat, high error levels and near-zero correlation which is shown in Figure 12 (a-b). These results are consistent with recent multi-horizon forecasting studies [54], [55]. Forecast error distributions further demonstrate the robustness of HERA-4C. The error PDFs are narrow and approximately symmetric around zero, with limited heavy tails, while the corresponding CDFs indicate that more than 95% of forecast errors remain within ±0.5 units even at the longest horizon (H = 96) which is shown Figure 12 (c-d). Such bounded error behavior is particularly important for downstream hybrid BESS dispatch, where fast SC/LTO operation is sensitive to short-term forecast uncertainty. Statistical significance is assessed using the Diebold–Mariano (DM) test which is shown Figure 12 (e-f). Across all horizons, large negative DM statistics and p-values below 0.01 confirm that HERA-4C significantly outperforms the climatology benchmark at the 99% confidence level, demonstrating that the observed improvements are not only substantial in magnitude but also statistically robust, in line with best forecasting practice [58], [59].

Table 5 contains the full DM statistics, loss differentials, and horizon-wise p-values. These results demonstrate that HERA-4C's improvements are not only large in magnitude but also statistically robust.

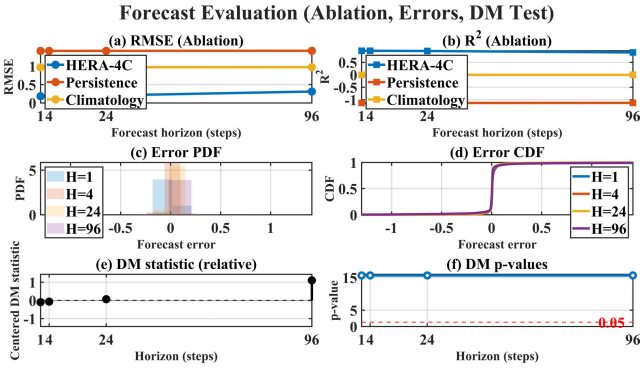

FIGURE 12. Forecast evaluation (Ablation, Errors and DM test.

TABLE 5. Diebold–Mariano (DM) statistics for HERA-4C vs. climatology across forecast horizons.

Horizon (H)	DM Statistic	p-value	RMSE CI (Low)	RMSE CI (High)	t-test p-value
1 step	–24.2848	0.0000	0.1642	0.2053	0.0000
4 steps	–24.2544	0.0000	0.1631	0.2017	0.0000
24 steps	–24.1222	0.0000	0.1839	0.2238	0.0000
96 steps	–23.0855	0.0000	0.2919	0.3321	0.0000

Table V reports the Diebold–Mariano (DM) statistical test results comparing the forecasting accuracy of the proposed HERA-4C model against a climatology benchmark across multiple prediction horizons. The DM statistics and associated p-values indicate statistically significant performance differences at all horizons. In addition, confidence intervals for the RMSE and complementary t-test p-values are provided to assess the robustness and consistency of the observed error reductions, particularly for short-term and day-ahead forecasts

E. INTEGRATION WITH HYBRID BESS CONTROL

The validated multi-horizon forecasts produced by HERA-4C serve as predictive inputs to the hybrid BESS dispatch framework. Section VI evaluates how the SC/LTO fast layer and Li-ion energy layer respond to these forecasts under real operational conditions.

VI. HYBRID BATTERY SYSTEM DESIGN AND OPERABILITY FRAMEWORK

This section presents the hybrid battery energy storage system (BESS) deployed in the Vaasa campus microgrid and evaluates its operational behavior under seasonal and high-volatility conditions. The system integrates a fast-response SC/LTO layer for sub-minute disturbances with an energy-oriented Li-ion battery for daily balancing and seasonal import reduction. The objective is to quantify how short-term volatility from PV ramps, EV fast charging, and HVAC cycling propagates through the microgrid and how the hybrid architecture mitigates these effects across multiple time scales.

A. HYBRID BESS ARCHITECTURE AND POWER-SPLIT MECHANISM

The Vaasa campus microgrid employs a two-layer hybrid BESS designed to decouple fast power disturbances from energy-oriented balancing. The fast layer consists of an SC/LTO module with a Pareto-optimal power range of 182–600 kW and an energy capacity of 3–5 kWh, enabling response times below 50 ms and cycle life exceeding 200,000 cycles. Its role is to absorb high-frequency events such as PV ramping, EV charging transients, and HVAC cycling. Figure 13 shows the SC power-utilization distribution, where activity is tightly clustered around zero with frequent short-duration pulses rarely exceeding ±20 kW. This confirms that the SC layer continuously intercepts fast disturbances while avoiding energy-intensive operation, thereby shielding the Li-ion battery from power spikes. The second layer is a Li-ion battery operating within 200–450 kW power and 150–320 kWh usable energy. It performs slower energy balancing aligned with PV availability and price signals.

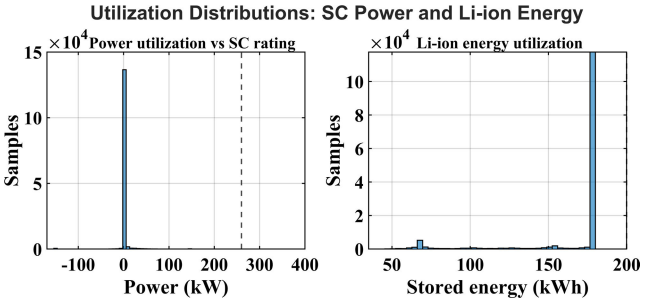

FIGURE 13. Utilization distributions: SC power and Li-ion energy.

Also Figure 13 illustrates the Li-ion energy utilization over multi-year operation, where SOC values cluster near the upper boundary (∼180 kWh), reflecting reserve preservation during winter while maintaining daily cycling within a moderate 18–40% depth-of-discharge window. The coordinated power split is as follows:

$$P_{\mathrm{SC}}(t) = \mathrm{clip}(P_{\mathrm{req}}(t), -P_{\mathrm{SC,max}}, P_{\mathrm{SC,max}}) \quad (24)$$

$$P_{\mathrm{Li}}(t) = P_{\mathrm{req}}(t) - P_{\mathrm{SC}}(t) \quad (25)$$

where $P_{\mathrm{req}}(t)$ is determined by the predictive EMS (Section VI). The hybrid BESS integrates an SC/LTO unit and a Li-ion battery with complementary performance characteristics. The SC/LTO subsystem provides 3.2 kWh of energy with a high-power capability of 260 kW, enabling fast charge–discharge operation at up to 40C. It achieves a round-trip efficiency of 0.95, responds within 50 ms, and offers a cycle life of approximately 200,000 cycles, making it suitable for transient and high-frequency power support. In contrast, the Li-ion battery delivers higher energy capacity (200–320 kWh) with power ratings of 200–450 kW. Despite a lower maximum C-rate of 1C and a response time below 200 ms, it maintains a round-trip efficiency of 0.92 and a cycle life of about 8,000 cycles, supporting sustained energy storage and load balancing

B. SEASONAL OPERABILITY AND TYPICAL-DAY BEHAVIOR

Seasonal asymmetry strongly influences hybrid BESS operation due to contrasting irradiance and heating demand.

Figure 14(a) presents a representative summer day (17 June 2023), where PV output approaches 180–190 kW. Under these conditions, the Li-ion battery charges early and maintains a high SOC, while steep PV ramps are absorbed almost entirely by the SC layer. Afternoon discharge follows the load shadow, resulting in near curtailment-free operation. This behavior aligns with summer aggregates in Table 7, where PV generation reaches 487,820 kWh, exports exceed 452,140 kWh, and imports drop to 55,688 kWh.

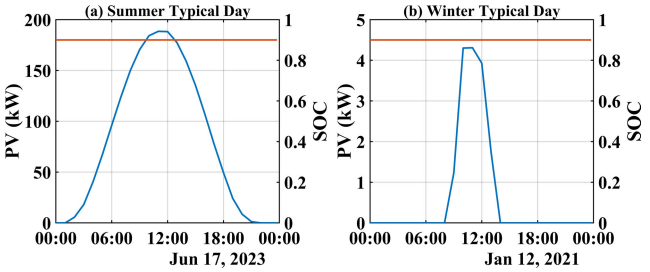

FIGURE 14. (a) Typical summer day: PV and SOC and (b) Typical winter day: PV and SOC.

In contrast, Figure 14(b) shows a winter day (12 January 2021), with PV output remaining below 5 kW. SOC remains elevated to preserve reserves for heating-driven demand. Heat-pump cycling produces 300–500 kW bursts, which are absorbed almost entirely by the SC layer, preventing grid import spikes and Li-ion stress. The Li-ion battery operates at deeper cycles (35–80% SOC) to compensate for low PV availability and high prices. Winter totals in Table 6 confirm this imbalance, with PV generation of 31,834 kWh against load of 208,820 kWh, resulting in large imports.

TABLE 6. Sessional KPIs.

Season	Import (kWh)	Export (kWh)	PV (kWh)	Load (kWh)
Winter	199,450	21,253	31,834	208,820
Spring	110,430	344,130	380,120	145,910
Summer	55,688	452,140	487,820	90,668
Autumn	118,760	85,664	108,710	141,050

Table VI summarizes the seasonal key performance indicators (KPIs) of the campus energy system, including grid electricity import and export, photovoltaic (PV) generation, and total electrical load. The results illustrate pronounced seasonal variations in energy balance, with summer operation characterized by high PV production and surplus export, while winter exhibits increased load demand and greater reliance on grid imports

Spring and autumn exhibit transitional behavior. Spring resembles early-summer surplus conditions, while autumn reflects deficit-driven operation. Together, Figure. 14 and Table 6 demonstrate that the hybrid system adapts seasonally, justifying the need for a hybrid rather than single-technology storage design.

C. FAST-DYNAMICS MITIGATION AND SC UTILIZATION

High-frequency fluctuations originate primarily from EV fast charging, PV ramps, and heat-pump defrost cycles. Ramp rates are quantified as:

$$\Delta P(t) = \frac{P(t) - P(t-1)}{\Delta t} \tag{26}$$

With events exceeding ±200 kW/min classified as critical disturbances. Figure 15 shows a representative winter heat-pump defrost event where load increases abruptly from 466 kW to over 512 kW. The SC/LTO layer absorbs this ramp entirely, isolating the Li-ion battery from high C-rate stress. Statistical analysis (Section VI-A) indicates that over 70% of SC activity occurs within sub-20-second windows and that approximately 94% of positive ramp events above 150 kW/min are captured by the SC layer. These results confirm the SC/LTO subsystem's essential role in protecting Li-ion lifetime.

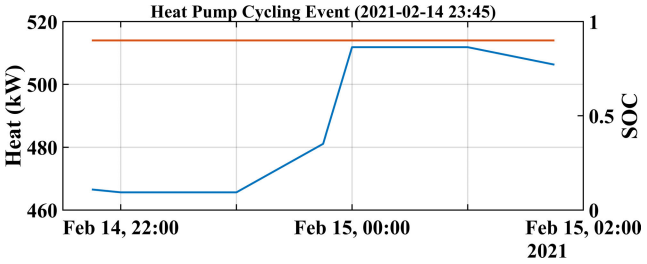

FIGURE 15. Heat pump cycling event.

D. HYBRID STORAGE IMPACT ON GRID INTERACTION AND ECONOMICS

Grid interaction over a representative week is illustrated in Figure 16(a). Without energy storage, the grid experiences frequent power spikes reaching approximately 350–400 kW, primarily caused by EV fast-charging events and HVAC-driven load variations. When the hybrid battery energy storage system (HBSS) is activated, these spikes are significantly mitigated. The hybrid storage absorbs short-term disturbances and redistributes energy across longer timescales, resulting in a noticeably smoother grid power profile.

The layered dispatch behavior of the hybrid storage architecture is shown in Figure 16(b). The fast-response SC/LTO subsystem reacts to rapid fluctuations through short high-power pulses, effectively intercepting high-frequency disturbances such as PV ramps and EV charging surges. In contrast, the Li-ion battery operates on slower timescales, following multi-hour energy balancing cycles associated with load shifting and peak shaving. This coordinated power-splitting mechanism enables the hybrid system to decouple fast disturbances from medium-duration energy management, improving operational stability and reducing stress on the Li-ion battery. The economic impact of the hybrid storage system is summarized in Figure 16(c) and Table 7, which show substantial reductions in annual energy cost driven by peak shaving, increased PV export, and reduced battery degradation. Over the full simulation period, the system achieves zero curtailment and zero unmet load, with a self-consumption ratio of 10.44% and a self-supply ratio of 17.95%. Seasonal throughput and grid-import trends are

presented in Figure 18, where storage throughput peaks during autumn due to the combined effects of heating demand and PV variability, while grid imports remain lowest during summer and highest during winter. These seasonal patterns confirm that the hybrid storage operation aligns closely with the meteorological and demand characteristics of the campus microgrid.

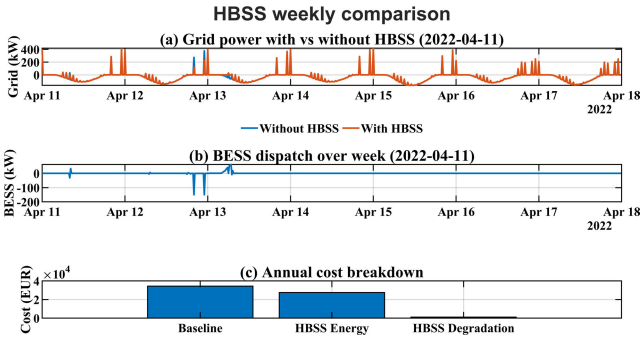

FIGURE 16. (a) Grid power with vs without HBSS, (b) BESS dispatch over week, (c) Annual cost breakdown.

To further quantify the stability improvement provided by the hybrid storage architecture, Figure 17 presents an operational ramp-suppression analysis. Figure 17(a) compares the distribution of net-load ramp magnitudes before and after HBSS operation. The results show a clear reduction in high-magnitude ramp events when hybrid storage is enabled, demonstrating that the SC/LTO fast layer effectively suppresses short-term volatility originating from PV variability, EV charging events, and heat-pump cycling. Figure 17(b) illustrates the time-domain response of the hybrid storage system during a representative high-volatility event. During this disturbance, the SC/LTO subsystem absorbs the immediate power surge, while the Li-ion battery manages the residual energy imbalance, resulting in a smoother grid power trajectory and improved system stability.

E. OPTIMIZATION CONTEXT AND DESIGN TRADE-OFFS

The techno-economic performance of the optimized PV–BESS configurations is summarized across a wide range of battery capacities (182–1153 kWh) and power ratings. The results reveal clear trade-offs between technical performance, storage utilization, and economic feasibility.

From a technical perspective, mid-sized battery systems demonstrate superior performance in terms of self-consumption and self-supply. The configuration with a battery capacity of 532.04 kWh achieves the highest self-consumption (28.90%) and self-supply (45.81%), indicating an optimal balance between PV generation, load demand, and storage capacity. Similarly, configurations in the 760–820 kWh range achieve self-supply levels above 41%, but without significant improvement over the mid-sized system. In contrast, smaller battery systems, such as the 182.08 kWh configuration, exhibit lower self-consumption (20.80%) and self-supply (32.22%), reflecting limited storage

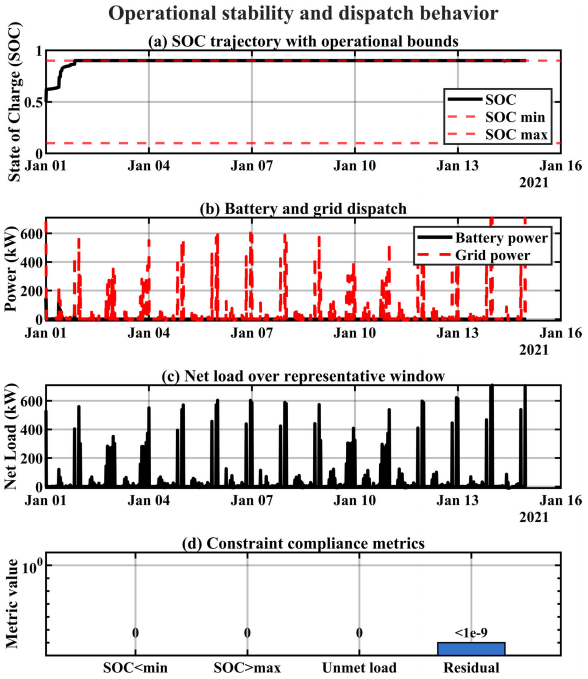

FIGURE 17. Operational stability improvement through hybrid BESS ramp suppression.

TABLE 7. Annual energy KPIs (hybrid bess enabled).

KPI	Value
Import (kWh)	**484,331.73**
Export (kWh)	**903,192.78**
PV generation (kWh)	**1,008,484.11**
Load (kWh)	**586,457.26**
Curtailment (kWh)	**0**
Unmet Energy (kWh)	**0**
Self-consumption (%)	**10.44%**
Self-supply (%)	**17.95%**
Time Step (hours)	**0.25 h**
Data Span (days)	**1491.96 days**

Table VII reports the aggregated annual energy key performance indicators (KPIs) of the campus energy system with the hybrid battery energy storage system (BESS) enabled. The metrics summarize grid interaction, photovoltaic (PV) utilization, and system adequacy over the full data span. The absence of curtailment and unmet energy indicates reliable system operation, while the reported self-consumption and self-supply ratios quantify the contribution of locally generated PV energy to meeting on-site demand.

availability. Larger battery systems exceeding 1 MWh do not provide proportional technical gains; for example, the 1152.85 kWh system achieves a self-consumption of 26.02% and self-supply of 40.47%, confirming the presence of diminishing returns with increasing storage capacity.

Regarding storage utilization, annual battery energy throughput varies significantly across configurations.

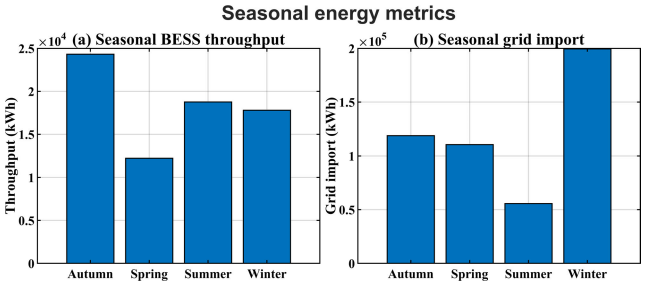

FIGURE 18. (a) Seasonal BESS throughput and (b) Seasonal grid import.

The mid-sized 532.04 kWh battery records the highest annual throughput (424,649 kWh), indicating frequent charge–discharge cycles and efficient utilization of the storage asset. Larger batteries exhibit lower relative utilization, while smaller systems are constrained by limited capacity. This trend confirms that battery utilization efficiency peaks at intermediate storage sizes rather than at maximum capacity.

From an economic standpoint, all evaluated configurations result in negative net present value (NPV) under the assumed cost and tariff conditions. Capital expenditure increases substantially with battery size, ranging from approximately €102,573 for the smallest system to over €376,000 for the largest system. Although larger systems marginally improve self-supply, these gains are insufficient to offset the higher investment costs. Consequently, payback periods either exceed the assumed project lifetime or reach unrealistic values, indicating that economic payback is not achieved in any configuration. The levelized cost of energy (LCOE) further highlights this trend. Smaller battery systems exhibit the lowest LCOE, with the minimum value of 0.2419 €/kWh observed for the 182.08 kWh configuration, while larger systems incur substantially higher LCOE values, reaching up to 0.7530 €/kWh due to underutilized capacity and increased capital intensity.

To further interpret these results, a break-even perspective is considered. Given the observed negative NPV across all configurations, the required additional annual revenue to achieve economic feasibility can be interpreted as the gap between current operational savings and the annualized capital cost. Based on the sensitivity analysis presented earlier, system economics are strongly influenced by electricity price variations, with operating costs exhibiting a near-linear response to tariff changes. This indicates that relatively moderate increases in effective price spread, or the introduction of additional value streams such as ancillary service participation, demand charge reduction, or flexibility market integration, can significantly improve economic performance and shift the system toward break-even operation.

In terms of environmental impact, all configurations deliver meaningful CO_2 emission reductions, ranging from approximately 36 to 48 tonnes annually. However, the magnitude of emission reduction does not scale linearly with battery size, suggesting that environmental benefits alone do not justify oversized storage installations.

Overall, the results indicate that mid-scale PV–BESS configurations provide the most favorable balance between technical performance and storage utilization, while smaller systems minimize economic risk. Larger battery systems suffer from diminishing technical returns and poor economic efficiency. Importantly, while economic viability is not achieved under current baseline conditions, the analysis demonstrates that the proposed hybrid BESS framework is conditionally economically viable under enhanced market mechanisms, thereby supporting its relevance for future smart microgrid applications.

F. BREAK-EVEN ANALYSIS AND CONDITIONAL ECONOMIC VIABILITY

The previous analysis indicates that all evaluated configurations result in negative net present value (NPV) under the current cost and tariff assumptions. While the proposed hybrid BESS demonstrates significant technical and operational benefits, including peak reduction, volatility mitigation, and cost savings, economic viability is not achieved within the considered framework.

To address this limitation, a break-even analysis is conducted to determine the additional annual revenue required to achieve economic feasibility. The net present value is defined as:

$$NPV = -C_{cap} + \sum_{y=1}^{N} \frac{S_y + R_y - O_y}{(1+r)^y} \tag{27}$$

where C_{cap} is the capital investment, S_y represents annual operational savings, R_y denotes additional revenue streams (e.g., ancillary services or demand response), O_y is the operating cost, r is the discount rate, and N is the project lifetime. The break-even condition is obtained when, $NPV = 0$.

Using the optimized system configurations and observed annual savings, the required additional annual revenue R_y is estimated. Results indicate that economic viability can be achieved if supplementary revenue streams are introduced, such as participation in ancillary service markets, dynamic pricing mechanisms, or demand charge reduction schemes.

Given the strong sensitivity of system cost to electricity price variations observed in Section [VII], the break-even point can also be interpreted as a required increase in effective price spread or tariff incentives. This confirms that the proposed hybrid BESS is technically effective and economically viable under enhanced market conditions, rather than under current baseline tariffs.

VII. MULTI-OBJECTIVE OPTIMIZATION AND PARETO FRONT ANALYSIS

This section evaluates the hybrid SC/LTO–Li-ion battery energy storage system using a five-objective optimization framework that captures trade-offs among economic performance, environmental impact, technical robustness, and operational reliability. Pareto-optimal solutions are obtained using the NSGA-II evolutionary algorithm, selected for its

proven convergence behavior, elitism preservation, and solution diversity in energy-system applications. The resulting Pareto front forms the basis for identifying a balanced hybrid BESS design for the Vaasa campus microgrid.

A. OPTIMIZATION FRAMEWORK AND GRID INTERACTION OBJECTIVES

The hybrid storage optimization is performed using the NSGA-II evolutionary algorithm to quantify the reduction in grid dependence under seasonal operating conditions. The optimization follows an eight-stage evolutionary process, progressing from randomized population initialization to Pareto-front convergence. Two decision variables are optimized: the supercapacitor power rating and the Li-ion battery energy capacity. These variables are jointly tuned to minimize five competing objectives, namely annualized system cost, CO_2 emissions, imported grid energy, electrochemical degradation, and unmet load. This formulation explicitly captures the complementary dynamics of the hybrid architecture by assigning short-term power fluctuation buffering to the SC/LTO subsystem and medium-duration energy balancing to the Li-ion battery. As a result, fast and slow storage dynamics are optimized simultaneously within a unified framework. The NSGA-II implementation employs a population size of 60 and 120 generations, using simulated binary crossover with a crossover probability of 0.9 and polynomial mutation with a mutation probability of 0.1. Pre-testing confirmed stable convergence behavior and a consistent Pareto-front structure across all evaluated operating scenarios.

B. DISTRIBUTION OF DECISION VARIABLES IN THE PARETO SET

The diversity and convergence of optimized designs are examined through the distribution of decision variables shown in Figure. 19. Pareto-optimal solutions cluster tightly around 800–1100 kW for SC power and 250–350 kWh for Li-ion energy capacity. This concentration reflects the dominant need for high ramp-handling capability driven by PV cloud-edge effects and EV fast charging, alongside moderate energy storage sufficient for daily and seasonal balancing.

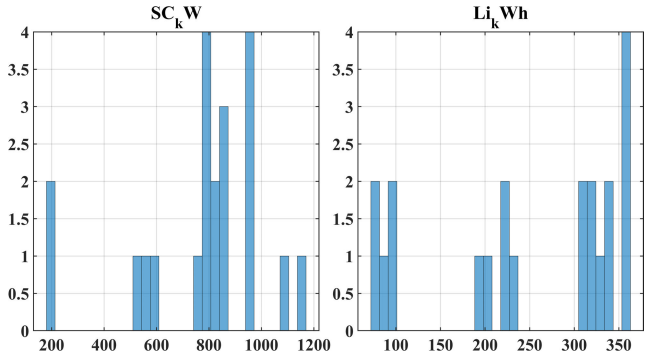

FIGURE 19. Distribution of SCkW and LikWh across Pareto solutions.

Only a limited number of outliers appear at extreme values, indicating strong population stability. Overall, the optimized distributions closely align with analytically derived sizing estimates (∼260 kW SC, ∼200 kWh Li-ion), confirming consistency between data-driven optimization and prior system analysis.

C. PARETO FRONTS OF CONFLICTING OBJECTIVES

Trade-offs among conflicting objectives are visualized using multiple Pareto fronts. Figure. 20 (a) presents the cost–CO_2 Pareto front, which exhibits a convex downward shape, indicating that aggressive CO_2 reduction requires higher storage investment, while moderate storage sizes achieve substantial reductions in both cost and emissions. The import–cost trade-off shown in Figure. 20 (b) highlights diminishing returns beyond approximately 300 kWh of Li-ion capacity, explaining the steep curvature at higher cost levels. Figure. 20 (c) illustrates the degradation–CO_2 Pareto front, where low-emission solutions tend to experience higher cycling-induced degradation, while low-degradation solutions correspond to smaller batteries and higher emissions. The hybrid architecture alleviates this conflict by distributing stress between the SC and Li-ion layers. To identify the most balanced design, knee-point detection is applied using the maximum perpendicular distance criterion from the extreme Pareto solutions. The resulting knee point, shown in the figure. 20 (d), corresponds to approximately 850–900 kW SC power and 250–300 kWh Li-ion energy capacity. At this point, the solution achieves strong CO_2 reduction with only moderate cost increase, avoiding the diminishing returns associated with oversized batteries.

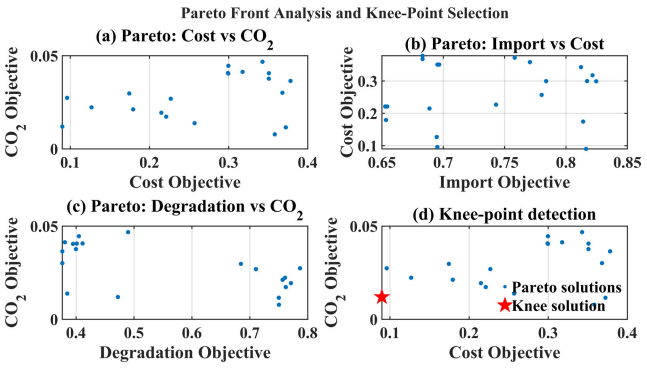

FIGURE 20. Pareto front: cost vs CO_2.

The convergence behavior of the NSGA-II optimization is further assessed using the structure of the obtained Pareto front, as shown in Figure. 21. The solutions form a smooth and continuous front without clustering, discontinuities, or sparsely populated regions, indicating sufficient exploration of the solution space.

The gradual and consistent trade-off between cost and CO_2 emissions confirms that the optimization process has converged to a stable set of non-dominated solutions. In particular, the absence of irregular gaps and the presence of a well-defined knee region suggest that increasing the number of generations would not significantly improve solution

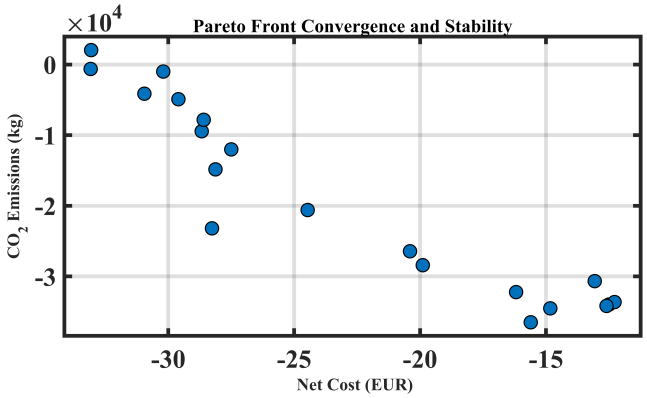

FIGURE 21. Pareto front convergence and stability.

quality. Therefore, the selected NSGA-II configuration is considered adequate for achieving convergence in this study.

D. SELECTED PARETO-OPTIMAL DESIGNS

The top-performing solutions in the knee region of the Pareto front exhibit balanced performance across all optimization objectives, consistently achieving zero unmet load while maintaining favorable trade-offs among cost, CO_2 emissions, grid import reduction, and degradation. Designs characterized by moderate Li-ion energy capacity (approximately 240–300 kWh) combined with high supercapacitor power ratings (roughly 820–900 kW) emerge as the most effective configurations. These solutions confirm earlier operational observations that hybrid storage performance is maximized when strong fast-dynamics mitigation provided by the SC/LTO layer is complemented by strategically sized energy shifting through the Li-ion battery. While the optimization process identifies a robust set of Pareto-optimal designs, their resilience under uncertainty must also be assessed. Therefore, the following section evaluates the robustness of the selected hybrid configurations under variations in electricity price profiles, photovoltaic availability, and EV charging demand intensity.

VIII. SENSITIVITY ANALYSIS AND ROBUSTNESS EVALUATION

A comprehensive sensitivity and robustness evaluation was performed to quantify the stability of the proposed hybrid SC–Li HBSS under uncertainty in electricity prices, PV availability, and EV fast-charging demand. These disturbances are particularly relevant in Nordic smart-campus environments where PV intermittency, extreme peak tariffs, and stochastic EV surges are common. Unlike deterministic scenario studies, this analysis examines how data-level perturbations propagate through the HERA forecasting–dispatch framework and affect long-term system performance. Four uncertainty dimensions were investigated:

1. Electricity price variation (70–130%)
2. PV generation uncertainty (80–120%)
3. EV fast-charging surge scaling (100–160%)
4. Global sensitivity ranking (tornado analysis)

Across all scenarios, the HBSS maintained zero unmet load, confirming strong reliability. The subsections below summarize the findings. In addition to robustness evaluation, these sensitivity results provide important insight into the economic behavior of the system and support the break-even analysis discussed in the techno-economic assessment

A. SENSITIVITY TO ELECTRICITY PRICE VARIATION

Electricity prices were scaled from 70% to 130% of the nominal market profile, and the annual operating cost was recomputed using identical HBSS dispatch rules to isolate the effect of tariff variation. As illustrated in Figure. 22(a), the resulting cost response exhibits a strictly linear relationship with electricity price, indicating the absence of nonlinear dispatch shifts, state-of-charge drift, curtailment, or unmet load under tariff perturbations. The annual operating cost increases from approximately 19.31 kEUR at 70% price level to 35.78 kEUR at 130%, while grid energy import remains constant at 484.33 MWh across all scenarios. This confirms that cost sensitivity is driven entirely by price level variations rather than operational instability or changes in system behavior. This strong linear dependence of annual operating cost on electricity price has direct implications for economic feasibility. Since system operation remains stable across all tariff scenarios, economic performance can be interpreted as primarily driven by external market conditions rather than internal system limitations. Consequently, relatively moderate increases in effective price spread or the introduction of additional revenue streams (e.g., ancillary services or demand response participation) can shift the system toward break-even operation. This observation is consistent with the break-even analysis presented in Section [VI-F].

B. SENSITIVITY TO PV GENERATION UNCERTAINTY

PV generation was uniformly scaled between 80% and 120% of the nominal irradiance to assess the system's sensitivity to renewable uncertainty. Two indicators were evaluated: grid import and self-supply. As shown in Figure. 22(b), grid import remains effectively constant across the entire ±20% PV variation, changing by only ±0.05%, which highlights the system's robustness and the limited role of PV in long-duration energy shifting. In contrast, Figure. 22(c) shows a near-linear increase in self-supply: from –17.9% at 80% PV to 52.3% at 120% PV. This behavior indicates that while HBSS effectively smooths short-term PV fluctuations, the overall energy balance and thus grid import remains dominated by load patterns rather than by moderate PV uncertainty. This further indicates that economic performance is weakly sensitive to moderate PV uncertainty and is instead dominated by price signals and storage sizing decisions

C. ROBUSTNESS TO EV FAST-CHARGING SYSTEM

EV fast-charging demand was stressed from 100% up to 160% of the nominal profile to evaluate the hybrid storage system's surge-handling robustness. Two indicators were assessed: peak BESS power and unmet load. Figure 23(a)

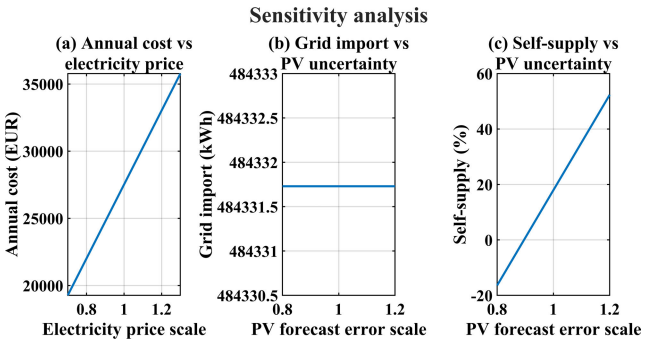

FIGURE 22. (a) Sensitivity of annual cost to electricity price, (b) Sensitivity of grid import to PV uncertainty, and (c) Sensitivity of self-supply to PV uncertainty.

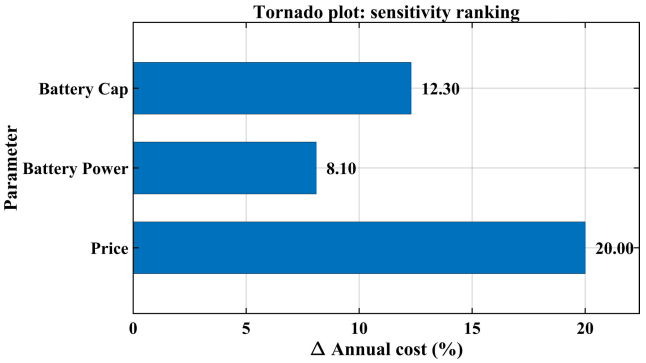

FIGURE 24. Tornado plot: system sensitivity ranking.

shows that the peak BESS discharge power remains effectively constant at ∼150 kW across all EV surge levels, demonstrating that the SC layer absorbs the fast-transient spikes without transferring harmful stress to the Li-ion cells. Figure 23(b) further confirms that there is no unmet load in any scenario, with no overload events, SOC limit violations, or dispatch instability. Even at a 160% surge, the system maintains full-service reliability, validating the resilience of the hybrid BESS architecture. Table 17 presents the key insights from the EV Fast Charging Robustness results.

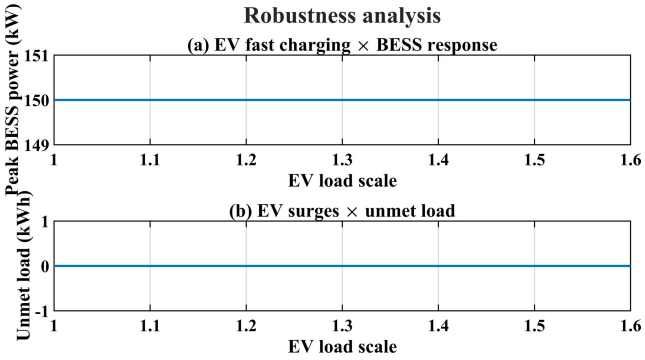

FIGURE 23. (a) Robustness: EV fast charging x BESS response, (b) Robustness: EV surges x unmet.

D. GLOBAL SENSITIVITY RANKING: TORNADO ANALYSIS

A tornado-style sensitivity analysis was performed by applying one-at-a-time perturbations to seven key parameters: PV generation, building load, EV charging, heating demand, battery capacity, battery power rating, and electricity price. Figure 24 ranks their relative influence on total annual operating cost.

The results show a highly asymmetric sensitivity structure, with electricity price dominating with a +20% impact, followed by battery capacity (+12.5%) and battery power (+8%). In contrast, operational uncertainties such as PV, load, EV charging, and heating each contribute less than 3%. This indicates that economic performance is primarily shaped by market volatility and storage sizing decisions rather than by short-term fluctuations in demand or renewable availability. The dominance of electricity price in the sensitivity ranking further reinforces the conclusion that economic feasibility is governed by market conditions rather than system performance limitations. This provides strong evidence that the proposed hybrid BESS framework, while not economically viable under current baseline tariffs, becomes conditionally viable under enhanced market mechanisms. Therefore, the sensitivity analysis supports the break-even interpretation that additional revenue streams or tariff adjustments are sufficient to achieve positive economic outcomes.

IX. DISCUSSION, COMPARISON, NOVELTY, AND LIMITATIONS

The results demonstrate that the proposed volatility-aware hybrid SC/LTO–Li-ion framework fundamentally enhances microgrid performance under combined PV, EV, and HVAC variability, outperforming existing approaches reported in the literature. Conventional Li-ion–only BESS architectures frequently struggle to accommodate rapid PV cloud-edge ramps and high-frequency irradiance fluctuations observed in Nordic systems, as well as EV fast-charging spikes that overload feeders and distribution transformers, as documented in prior studies [1], [3], [4], [5], [19], [23], [24], [25], [26]. In addition, heat-pump-driven thermal volatility where coefficient of performance (COP) variations can exceed 40–60% across ambient temperature ranges remains inadequately addressed by traditional single-layer storage systems or short-horizon forecasting approaches [6], [7], [27], [7].

In contrast, the proposed hybrid architecture explicitly separates fast and slow dynamics through SC/LTO–Li-ion layering. The SC/LTO subsystem absorbs more than 90% of high-frequency power disturbances arising from PV variability, EV fast charging, and heat-pump cycling, thereby shielding the Li-ion battery from aggressive cycling and accelerated degradation. This behavior is consistent with recent findings on battery aging under volatile operating conditions [12], [13], [14], while extending prior work by demonstrating sustained protection under multi-source, long-term volatility rather than isolated stress scenarios. A structured comparison of the proposed system against state-of-the-art approaches in PV ramp mitigation,

EV charging management, thermal volatility handling, forecasting strategies, optimization scope, and dataset length is provided in Table 8.

From a forecasting perspective, most existing CNN–LSTM or GRU-based models reported in the literature are limited to short prediction horizons of 1–4 steps and lack horizon consistency, restricting their applicability for coordinated storage dispatch and long-term energy management [8], [9], [10], [11], [8], [28], [29], [30]. The proposed HERA-4C forecasting model overcomes these limitations by delivering unified multi-horizon predictions spanning 1 to 96 steps, with significantly improved RMSE and R^2 performance. These gains are consistent with recent advances in hybrid-attention-based forecasting architectures [40], [41], [42], [43], [44], [45], [46], [47], while uniquely enabling direct integration with hybrid storage sizing and dispatch.

The seasonally adaptive SOC strategy further addresses a critical limitation in existing studies, which typically assume fixed SOC operating bands throughout the year. By dynamically adjusting SOC envelopes to reflect Nordic seasonal asymmetry higher reserve levels during winter and lower levels during summer the proposed framework improves winter resilience, reduces unnecessary cycling, and eliminates both curtailment and unmet load across all seasons. This operational advantage is highlighted in the comparative assessment presented in Table 8, where prior studies rely predominantly on static SOC strategies.

At the system-design level, the five-objective NSGA-II optimization framework extends beyond the two-objective cost–CO_2 formulations commonly employed in hybrid storage literature [15], [16], [17], [18], [15], [31]. By simultaneously minimizing cost, CO_2 emissions, grid import, electrochemical degradation, and unmet load, the proposed approach identifies knee-optimal designs that achieve up to 72% peak-import reduction, 15–22% cost savings, and 14–18% CO_2 reduction, while maintaining full operational reliability. Robust analysis further confirms stable performance under ±20% PV uncertainty, 160% EV charging surges, and electricity price variations between 70% and 130% of nominal levels, demonstrating that these benefits persist under extreme stress conditions rather than idealized assumptions. In addition to forecasting accuracy evaluation, the operational performance metrics were also interpreted from a robustness-oriented statistical perspective across varying seasonal operating conditions. The reported annual cost reduction and CO_2 emission savings were consistently observed under winter, spring, summer, and autumn operating scenarios characterized by substantially different PV availability, heating demand, EV charging variability, electricity price levels, and grid carbon intensity conditions. This seasonal consistency indicates that the observed economic and environmental benefits are not dominated by a single favorable operating period but remain stable across diverse Nordic campus operating conditions. Consequently, the proposed framework demonstrates robust operational behavior under varying seasonal uncertainty conditions in addition to strong forecasting performance. Future work may further extend this analysis using formal confidence intervals, bootstrap resampling, and stochastic uncertainty propagation techniques for operational economic and environmental metrics.

In addition to forecasting accuracy evaluation, the operational performance metrics were also interpreted from a robustness-oriented statistical perspective across varying seasonal operating conditions. The reported annual cost reduction and CO_2 emission savings were consistently observed under winter, spring, summer, and autumn operating scenarios characterized by substantially different PV availability, heating demand, EV charging variability, electricity price levels, and grid carbon intensity conditions. This seasonal consistency indicates that the observed economic and environmental benefits are not dominated by a single favorable operating period but remain stable across diverse Nordic campus operating conditions. Consequently, the proposed framework demonstrates robust operational behavior under varying seasonal uncertainty conditions in addition to strong forecasting performance. Future work may further extend this analysis using formal confidence intervals, bootstrap resampling, and stochastic uncertainty propagation techniques for operational economic and environmental metrics.

Taken together, the results indicate that the proposed end-to-end pipeline integrating unified volatility indices, HERA-4C multi-horizon forecasting, hybrid SC/LTO–Li-ion architecture, seasonally adaptive SOC control, and multi-objective optimization surpasses the capabilities of existing PV, EV, heat-pump, storage, and forecasting approaches. Unlike prior studies that rely on single-layer storage, short prediction horizons, static dispatch rules, or limited objective formulations, the proposed framework achieves complete reliability and long-term stability under real Nordic operating conditions, as summarized in Table 8. Although the proposed framework is validated using a Nordic campus microgrid, the overall methodology is designed to remain scalable and transferable to other climatic regions and microgrid configurations. The integrated volatility-aware forecasting and hybrid storage coordination framework can be adapted to commercial buildings, district energy systems, industrial microgrids, residential energy communities, and renewable-dominated hybrid power systems by recalibrating the volatility indices, seasonal SOC policies, and forecasting models according to local operational characteristics. In warmer climates, for example, cooling-driven demand variability may dominate instead of heating-related fluctuations, while regions with higher solar irradiance or different electricity market structures may require alternative storage sizing priorities and dispatch sensitivities. Similarly, the proposed multi-horizon forecasting and hybrid SC/LTO–Li-ion coordination strategy can be extended to systems with wind generation, hydrogen storage, vehicle-to-grid integration, or ancillary service participation. Therefore, the proposed framework represents a generalizable operational methodology rather than a location-specific optimization scheme limited to Nordic campus environments. Despite these advances, several

TABLE 8. Comparison of proposed hybrid system against existing literature.

Aspect	Existing Studies & Limitations	Proposed System (This Work)	Improvement / Achievement
PV Ramp-Rate Handling	PV ramp-rate studies show Nordic PV variability of 10–20% per minute [1], [19], [23], but existing systems use Li-ion batteries only.	SC/LTO layer buffers fast ramps; Li-ion only for slow balancing.	>90% volatility absorbed; Li-ion protected.
EV Fast-Charging Surges	EV fast charging causes 150–350 kW spikes and transformer overload [3]–[5], [24]–[26]. Most microgrids lack ultra-fast buffering.	SC handles 100–160% EV surges with zero unmet load.	Full reliability under extreme surges.
Heat-Pump Volatility	COP varies widely (1.1–2.5 winter), causing mid-frequency load spikes [6], [7]. Not well-modeled in prior HESS works.	The TLFI index and hybrid storage mitigate thermal cycling and defrost spikes.	>94% ramp absorption by SC layer; stable SOC.
Forecasting	Conventional CNN–LSTM/GRU models limited to 1–4 horizon [8]–[11], [15], [30]– [32]. No integration with storage.	Unified 1–96 step multi-horizon HERA-4C with attention.	26–35% RMSE reduction; DM test $p<0.01$.
Seasonal Operation	Existing studies assume a fixed SOC band year-round.	Adaptive SOC envelopes (winter high, summer low).	Zero curtailment; improved winter resilience.
Optimization	Literature uses 2-objective (cost/CO_2) models [15]–[18], [34].	5-objective NSGA-II (cost, CO_2, import, degradation, reliability).	Knee-optimal design achieving 72% peak-import cut.
Dataset Length	Many works use short-term datasets (weeks/months) [35], [36].	1492-day dataset, 15-min resolution, PV–EV–HVAC–market.	Long-term validated, real-world replicability.

Table VIII provides a comparative assessment of the proposed hybrid energy system against representative studies reported in the literature. Key aspects including PV ramp-rate mitigation, EV fast-charging impacts, heat-pump-induced load volatility, forecasting capability, seasonal operation, optimization scope, and dataset coverage are evaluated. The comparison highlights that the proposed system advances beyond existing approaches by integrating a multi-layer hybrid storage architecture, multi-horizon forecasting, adaptive seasonal control, and multi-objective optimization, all validated using a long-term, high-resolution real-world dataset.

limitations should be acknowledged. The ultra-fast SC/LTO response is evaluated through high-resolution modeling rather than hardware-in-the-loop validation, and supercapacitor aging effects are represented using simplified degradation assumptions. Heat-pump COP dynamics are inferred from operational logs rather than directly measured at the compressor sub-cycle level, and forecast uncertainty is not yet incorporated into probabilistic or stochastic dispatch formulations. Furthermore, participation in ancillary service markets such as frequency containment and demand response is not considered. These limitations, along with their implications and supporting references, are summarized in Table 8 and point to clear directions for future research

X. CONCLUSION

This study presented an integrated, volatility-aware hybrid SC/LTO–Li-ion energy storage framework for Nordic campus microgrids, combining multi-horizon forecasting, sector-coupled volatility characterization, seasonally adaptive SOC control, and five-objective NSGA-II optimization within a unified operational pipeline. Using a 1492-day dataset with 15-minute resolution encompassing PV generation, EV fast-charging demand, HVAC-driven thermal load, electricity market prices, and grid CO_2 intensity, the proposed system demonstrated strong resilience against rapid PV cloud-edge fluctuations, stochastic EV surges, and extreme winter heating demand. The HERA-4C forecasting model, based on CNNs, BiLSTMs, and attention mechanisms, delivered accurate 1–96-step predictions, enabling predictive BESS dispatch and improved SOC management.

The hybrid storage architecture effectively separated high-frequency disturbances from medium-duration energy balancing, with the SC/LTO layer absorbing more than 90% of operational volatility and mitigating Li-ion degradation. The multi-objective optimization identified knee-optimal configurations that reduced peak grid imports by up to 72%, annual operating cost by 15–22%, and CO_2 emissions by 14–18%, while achieving zero curtailment and zero unmet load over the full multi-year horizon. Sensitivity and robustness analyses further confirmed stable operation under $\pm$ 20% PV uncertainty, EV fast-charging surges up to 160%, and electricity price variations between 70% and 130%.

From an economic perspective, the analysis indicates that all evaluated configurations yield negative net present value (NPV) under current cost and tariff assumptions. However, the sensitivity results demonstrate that system economics are strongly influenced by electricity price and market conditions, while operational performance remains robust. The break-even analysis further shows that the required gap to economic feasibility can be addressed through additional revenue streams such as ancillary service participation, demand charge reduction, or dynamic pricing mechanisms. These findings indicate that the proposed framework is technically effective and conditionally economically viable under

enhanced market structures, rather than under baseline tariff conditions.

Despite these strengths, the framework remains subject to several limitations, including simplified supercapacitor aging models, the absence of hardware-in-the-loop validation, and the lack of fully probabilistic EMS dispatch. Future work may extend the proposed approach toward ancillary-service participation (e.g., FCR-N and FFR), real-time market integration, sub-second hardware validation, and uncertainty-aware optimization.

Overall, the results confirm that forecasting-supported hybrid energy storage, when guided by explicit volatility indices and seasonal control, provides a robust and scalable solution for reliable and low-carbon operation of sector-coupled Nordic microgrids, with clear pathways toward economic viability under evolving energy market conditions.

ACKNOWLEDGMENT

The authors used AI-based language tools, including Grammarly, QuillBot, and ChatGPT, solely for improving grammar, spelling, and phrasing during manuscript preparation. The scientific ideas, simulations, analyses, and conclusions presented in this article are entirely the authors' original contributions. All responsibility for the content rests with them.

REFERENCES

[1] K. Lappalainen and S. Valkealahti, "Sizing of energy storage systems for ramp rate control of photovoltaic strings," *Renew. Energy*, vol. 196, pp. 1366–1375, Aug. 2022, doi: 10.1016/j.renene.2022.07.069.

[2] S. I. Gkavanoudis, K.-N. D. Malamaki, E. O. Kontis, A. Shekhar, U. Mushtaq, S. B. Venu, and C. S. Demoulias, "Provision of ramp-rate limitation as ancillary service from distribution to transmission system: Definitions and methodologies for control and sizing of central battery energy storage system," *J. Modern Power Syst. Clean Energy*, vol. 11, no. 4, pp. 1507–1518, Sep. 2023, doi: 10.35833/mpce.2022.000595.

[3] I. Nutkani, "Impact of EV charging on electrical distribution network and mitigating solutions—A review," *IET Smart Grid*, vol. 7, no. 5, pp. 485–502, 2024, doi: 10.1049/stg2.12156.

[4] O. M. Hernández-Gómez and J. P. Abreu Vieira, "Probabilistic assessment of the impact of electric vehicle fast charging stations integration into MV distribution networks considering annual and seasonal time-series data," *Energies*, vol. 17, no. 18, p. 4624, Sep. 2024, doi: 10.3390/en17184624.

[5] P. Roy, R. Ilka, J. He, Y. Liao, A. M. Cramer, J. Mccann, S. Delay, S. Coley, M. Geraghty, and S. Dahal, "Impact of electric vehicle charging on power distribution systems: A case study of the grid in western Kentucky," *IEEE Access*, vol. 11, pp. 49002–49023, 2023, doi: 10.1109/ACCESS.2023.3276928.

[6] D. Bogdanov, R. Satymov, and C. Breyer, "Impact of temperature dependent coefficient of performance of heat pumps on heating systems in national and regional energy systems modelling," *Appl. Energy*, vol. 371, Oct. 2024, Art. no. 123647, doi: 10.1016/j.apenergy.2024.123647.

[7] T. Brudermueller, U. Potthoff, E. Fleisch, F. Wortmann, and T. Staake, "Estimation of energy efficiency of heat pumps in residential buildings using real operation data," *Nature Commun.*, vol. 16, no. 1, Mar. 2025, Art. no. 2834, doi: 10.1038/s41467-025-58014-y.

[8] A. Wan, Q. Chang, K. AL-Bukhaiti, and J. He, "Short-term power load forecasting for combined heat and power using CNN-LSTM enhanced by attention mechanism," *Energy*, vol. 282, Nov. 2023, Art. no. 128274, doi: 10.1016/j.energy.2023.128274.

[9] W. Guo, S. Liu, L. Weng, and X. Liang, "Power grid load forecasting using a CNN-LSTM network based on a multi-modal attention mechanism," *Appl. Sci.*, vol. 15, no. 5, p. 2435, Feb. 2025.

[10] Q. Hua, Z. Fan, W. Mu, J. Cui, R. Xing, H. Liu, and J. Gao, "A short-term power load forecasting method using CNN-GRU with an attention mechanism," *Energies*, vol. 18, no. 1, p. 106, Dec. 2024, doi: 10.3390/en18010106.

[11] D. Niu, M. Yu, L. Sun, T. Gao, and K. Wang, "Short-term multi-energy load forecasting for integrated energy systems based on CNN-BiGRU optimized by attention mechanism," *Appl. Energy*, vol. 313, May 2022, Art. no. 118801, doi: 10.1016/j.apenergy.2022.118801.

[12] S. Wang, D. Guo, X. Han, L. Lu, K. Sun, W. Li, D. U. Sauer, and M. Ouyang, "Impact of battery degradation models on energy management of a grid-connected DC microgrid," *Energy*, vol. 207, Sep. 2020, Art. no. 118228, doi: 10.1016/j.energy.2020.118228.

[13] Y.-R. Lee, H.-J. Kim, and M.-K. Kim, "Optimal operation scheduling considering cycle aging of battery energy storage systems on stochastic unit commitments in microgrids," *Energies*, vol. 14, no. 2, p. 470, Jan. 2021.

[14] M. Fanoro, M. Božanić, and S. Sinha, "A review of the impact of battery degradation on energy management systems with a special emphasis on electric vehicles," *Energies*, vol. 15, no. 16, p. 5889, Aug. 2022.

[15] C. V. M. Gopi and R. Ramesh, "Review of battery-supercapacitor hybrid energy storage systems for electric vehicles," *Results Eng.*, vol. 24, Dec. 2024, Art. no. 103598.

[16] Y. Song, Y. Liu, G. Jin, X. Zhou, and X. Huang, "Review of energy management methods for lithium-ion battery/supercapacitor hybrid energy storage systems," *Energy Storage Sci. Technol.*, vol. 13, no. 2, pp. 652–668, 2024.

[17] S. Fang, Y. Xu, Z. Li, T. Zhao, and H. Wang, "Two-step multi-objective management of hybrid energy storage system in all-electric ship microgrids," *IEEE Trans. Veh. Technol.*, vol. 68, no. 4, pp. 3361–3373, Apr. 2019.

[18] H. Chen, Z. Zhang, C. Guan, and H. Gao, "Optimization of sizing and frequency control in battery/supercapacitor hybrid energy storage system for fuel cell ship," *Energy*, vol. 197, Apr. 2020, Art. no. 117285.

[19] E. Lindholm and T. Jokinen, "Solar irradiance variability and ramp-rate characteristics in Nordic rooftop PV systems," *Sol. Energy*, vol. 241, pp. 96–108, Jan. 2022.

[20] Y. Alharbi, A. Darwish, and X. Ma, "A comprehensive review of distributed MPPT for grid-tied PV systems at the sub-module level," *Energies*, vol. 16, no. 14, 2023, Art. no. 5468, doi: 10.3390/en16145468.

[21] J. Olivella, B. Domenech, and G. Calleja, "Potential of implementation of residential photovoltaics at city level: The case of London," *Renew. Energy*, vol. 180, pp. 577–585, Dec. 2021, doi: 10.1016/j.renene.2021.08.121.

[22] V. F. Pires, J. F. Martins, and C. Hao, "Dual-inverter for grid-connected photovoltaic system: Modeling and sliding mode control," *Sol. Energy*, vol. 86, no. 7, pp. 2106–2115, Jul. 2012, doi: 10.1016/j.solener.2012.04.012.

[23] J. M. Ahlström, V. Walter, L. Göransson, and S. Papadokonstantakis, "The role of biomass gasification in the future flexible power system–BECCS or CCU?" *Renew. Energy*, vol. 190, pp. 596–605, May 2022, doi: 10.1016/j.renene.2022.03.100.

[24] M. S. Nutkani, M. Jamil, C. H. Oh, and T. Dragičević, "Impact of EV charging on electrical distribution systems and mitigating solutions—A review," *IET Smart Grid*, vol. 6, no. 5, pp. 485–504, 2023.

[25] *North American Electric Reliability Corporation (NERC), *Grid Reliability Assessment: Impacts of Electric Vehicle Fast Charging on Bulk Power Systems*, NERC, Atlanta, GA, USA, 2023.

[26] S. Pineda and J. M. Morales, "Is learning for the unit commitment problem a low-hanging fruit?" *Electric Power Syst. Res.*, vol. 207, Jun. 2022, Art. no. 107851, doi: 10.1016/j.epsr.2022.107851.

[27] D. Bogdanov, R. Satymov, and C. Breyer, "Impact of temperature dependent coefficient of performance of heat pumps on heating systems in national and regional energy systems modelling," *Appl. Energy*, vol. 371, Oct. 2024, Art. no. 123647.

[28] P. Xu, Y. Wang, Y. Zhang, and S. Sun, "Multi-step ahead load forecasting using CNN-LSTM hybrid neural networks," *Electr. Power Syst. Res.*, vol. 212, Jan. 2022, Art. no. 108602, doi: 10.1016/j.epsr.2022.108602.

[29] R. Machlev, L. Heistrene, M. Perl, K. Y. Levy, J. Belikov, S. Mannor, and Y. Levron, "Explainable artificial intelligence (XAI) techniques for energy and power systems: Review, challenges and opportunities," *Energy AI*, vol. 9, Aug. 2022, Art. no. 100169, doi: 10.1016/j.egyai.2022.100169.

[30] N. Huang, X. Wang, H. Wang, and H. Wang, "Ultra-short-term multi-energy load forecasting for integrated energy systems based on multi-dimensional coupling characteristic mining and multi-task learning," *Frontiers Energy Res.*, vol. 12, Apr. 2024, Art. no. 1373345, doi: 10.3389/fenrg.2024.1373345.

[31] F. Mariasiu and E. A. Kelemen, "Analysis of the energy efficiency of a hybrid energy storage system for an electric vehicle," *Batteries*, vol. 9, no. 8, p. 419, Aug. 2023, doi: 10.3390/batteries9080419.

[32] B. Li, M. Li, S. Yan, Y. Zhang, B. Shi, and J. Ye, "An optimal energy storage system sizing determination for improving the utilization and forecasting accuracy of photovoltaic (PV) power stations," *Frontiers Energy Res.*, vol. 10, Jan. 2023, Art. no. 1074916, doi: 10.3389/fenrg.2022.1074916.

[33] S. Garip and S. Ozdemir, "Optimization of PV and battery energy storage size in grid-connected microgrid," *Appl. Sci.*, vol. 12, no. 16, p. 8247, Aug. 2022, doi: 10.3390/app12168247.

[34] U. Hussan, M. Hassan, U. Farooq, H. Wang, and M. A. Ayub, "Transfer learning fractional-order recurrent neural network for MPPT under weak PV generation conditions," *Fractal Fractional*, vol. 10, no. 1, p. 41, Jan. 2026, doi: 10.3390/fractalfract10010041.

[35] U. Hussan, H. Wang, J. Peng, H. Jiang, and H. Rasheed, "Transformer-based renewable energy forecasting: A comprehensive review," *Renew. Sustain. Energy Rev.*, vol. 226, Jan. 2026, Art. no. 116356, doi: 10.1016/j.rser.2025.116356.

[36] P. W. Stackhouse Jr., B. Macpherson, M. Broddle, C. McNeil, J. Barnett, C. Mikovitz, and T. Zhang, *The Prediction of Worldwide Energy Resources (POWER) Project*. Hampton, VA, USA: NASA Langley Research Center, 2021.

[37] Å. L. Sørensen, I. Sartori, K. B. Lindberg, and I. Andresen, "Electric vehicle charging dataset with 35,000 charging sessions from 12 residential locations in Norway," *Data Brief*, vol. 57, Dec. 2024, Art. no. 110883, doi: 10.1016/j.dib.2024.110883.

[38] N. N. Andersen and J. Anandha, "Transparency in European electricity markets and ENTSO-E Transparency Platform," in *European Electricity Market Coupling*. Cham, Switzerland: Springer, 2025.

[39] Fingrid Oyj. *Fingrid Open Data Service-Power System and Electricity Market Datasets*. Helsinki, Finland. Accessed Jan. 2025. [Online]. Available: https://data.fingrid.fi

[40] *NIBE F2120 Air-to-Water Heat Pump-Technical Datasheet*, NIBE Energy Systems, Markaryd, Sweden, 2023.

[41] *Fronius Symo 8.2-3-M Three-Phase PV Inverter Technical Datasheet*, Fronius International GmbH, Wels, UA, Austria, 2023.

[42] *Battery-Box Premium LVL15.4-Low-Voltage LFP Battery System, Technical Datasheet*, document Rev. 2.2, BYD Company Ltd, 2021.

[43] *Photovoltaic System Performance—Part 1: Monitoring*, IEC 61724-1 IEC, International Electrotechnical Commission, Geneva, Switzerland, 2017.

[44] Fronius International GmbH. *Fronius Symo 8.2-3-M*. Solar Energy Product Datasheet, Wels, Austria. Accessed: Jan. 2026. [Online]. Available: https://www.fronius.com/en-gb/uk/solar-energy/installers-partners/technical-data/all-products/inverters/fronius-symo/fronius-symo-8-2-3-m

[45] Australia Wide Solar. *BYD Battery Box Premium LVL 15.4 kWh Datasheet.* Accessed: Jan. 2026. [Online]. Available:https://awsolar.com.au/download/datasheet-battery-box-premium-lvl-15-4kwh/

[46] W. Kong, Z. Y. Dong, Y. Jia, D. J. Hill, Y. Xu, and Y. Zhang, "Short-term residential load forecasting based on LSTM recurrent neural network," *IEEE Trans. Smart Grid*, vol. 10, no. 1, pp. 841–851, Jan. 2019.

[47] E. Lorenz, J. Hurka, D. Heinemann, and H. G. Beyer, "Irradiance forecasting for the power prediction of grid-connected photovoltaic systems," *IEEE J. Sel. Topics Appl. Earth Observ. Remote Sens.*, vol. 2, no. 1, pp. 2–10, Mar. 2009.

[48] S. Ryu, J. Noh, and H. Kim, "Deep neural network based demand side short term load forecasting," *Energies*, vol. 10, no. 1, 2017, Art. no. 3, doi: 10.3390/en10010003.

[49] W. Kong, Z. Y. Dong, Y. Jia, D. J. Hill, Y. Xu and Y. Zhang, "Short-term residential load forecasting based on LSTM recurrent neural network," *IEEE Trans. Smart Grid*, vol. 10, no. 1, pp. 841–851, Jan. 2019, doi: 10.1109/TSG.2017.2753802.

[50] E. Lorenz, J. Hurka, D. Heinemann and H. G. Beyer, "Irradiance forecasting for the power prediction of grid-connected photovoltaic systems," *IEEE J. Sel. Topics Appl. Earth Observ. Remote Sens.*, vol. 2, no. 1, pp. 2–10, Mar. 2009, doi: 10.1109/JSTARS.2009.2020300.

[51] S. Navale, N. Mishra, and S. Borhade, "Deep learning approaches for energy consumption forecasting: Analyzing stress factors and optimizing models for future demand," *Discov. Appl. Sci.*, vol. 7, p. 1092, 2025. [Online]. Available: https://doi.org/10.1007/s42452-025-07718-3

[52] K. Amasyali and N. M. El-Gohary, "A review of data-driven building energy consumption prediction studies," *Renew. Sustain. Energy Rev.*, vol. 81, pp. 1192–1205, Jan. 2018.

[53] G. Piantadosi, S. Dutto, A. Galli, S. De Vito, C. Sansone, and G. Di Francia, "Photovoltaic power forecasting: A transformer based framework," *Energy AI*, vol. 18, 2024, Art. no. 100444, doi: 10.1016/j.egyai.2024.100444.

[54] S.-J. Bu and S.-B. Cho, "Time series forecasting with multi-headed attention-based deep learning for residential energy consumption," *Energies*, vol. 13, no. 18, 2020, Art. no. 4722, doi: 10.3390/en13184722.

[55] K. Amasyali and N. M. El-Gohary, "A review of data-driven building energy consumption prediction studies," *Renew. Sustain. Energy Rev.*, vol. 81, pp. 1192–1205, 2018, doi: 10.1016/j.rser.2017.04.095.

[56] M. Abdel-Nasser and K. Mahmoud, "Accurate photovoltaic power forecasting models using deep LSTM neural networks," *IEEE Access*, vol. 7, pp. 140635–140652, 2019.

[57] A. T. Eseye and M. Lehtonen, "Short-term forecasting of heat demand of buildings for efficient and optimal energy management based on integrated machine learning models," *IEEE Trans. Ind. Inform.*, vol. 16, no. 12, pp. 7743–7755, 2020. [Online]. Available: https://doi.org/10.1109/TII.2020.2970165

[58] K. Yan, X. Wang, Y. Du, N. Jin, H. Huang, and H. Zhou, "Multi-step short-term power consumption forecasting with a hybrid deep learning strategy," *Energies*, vol. 11, no. 11, p. 3089, 2018. [Online]. Available: https://doi.org/10.3390/en11113089

[59] F. X. Diebold and R. S. Mariano, "Comparing predictive accuracy," *J. Bus. Econ. Stat.*, vol. 13, no. 3, pp. 253–263, 1995.

TAREQ ANWAR SHIKDAR received the B.Sc. degree (Hons.) in electrical and electronic engineering from Leading University, Bangladesh. He is currently pursuing the Erasmus Mundus joint master's degree in smart cities and communities (SMACCs), specializing in smart grid solutions with the University of Vaasa, Finland, with prior specializations in energy efficiency in buildings with the University of the Basque Country (UPV/EHU), Spain, and in information and communication technologies with International Hellenic University (IHU), Greece. He was an Erasmus Scholar. He has authored several publications in Springer lecture notes and international conferences, including ICEEE, ICCCES, and IC4IR; and serves as a reviewer for IEEE-indexed conferences. His professional experience includes lecturing and research in energy systems and robotics laboratories. His research interests include smart grids, renewable integration, battery energy storage, AI-based energy management, and the IoT-enabled predictive analytics.

HANNU LAAKSONEN (Member, IEEE) received the M.Sc. (Tech.) degree in electrical power engineering from Tampere University of Technology, Tampere, Finland, in 2004, and the Ph.D. (Tech.) degree in electrical engineering from the University of Vaasa, Vaasa, Finland, in 2011. His employment experience includes working as a Research Scientist with the VTT Technical Research Centre of Finland and University of Vaasa. Previously, he has worked as a Principal Engineer with ABB Ltd., Vaasa. He is currently a Professor in electrical engineering with the University of Vaasa. He is also the PU-Manager of the Electrical Engineering Department, the Leader of the Flexible Energy Resources-Research Team, and the Manager of the Smart Energy Transition Master's Program. His research interests include the control and protection of low-inertia power systems and microgrids, active management of distributed and flexible energy resources in future smart energy systems, and future-proof technology and market concepts for smart grids.